

Electronic Theses and Dissertations, 2004-2019

2014

Decentralized Power Management and Transient Control in Hybrid Fuel Cell Ultra-Capacitor System

Seyed Omid Madani
University of Central Florida

 Part of the [Mechanical Engineering Commons](#)
Find similar works at: <https://stars.library.ucf.edu/etd>
University of Central Florida Libraries <http://library.ucf.edu>

This Doctoral Dissertation (Open Access) is brought to you for free and open access by STARS. It has been accepted for inclusion in Electronic Theses and Dissertations, 2004-2019 by an authorized administrator of STARS. For more information, please contact STARS@ucf.edu.

STARS Citation

Madani, Seyed Omid, "Decentralized Power Management and Transient Control in Hybrid Fuel Cell Ultra-Capacitor System" (2014). *Electronic Theses and Dissertations, 2004-2019*. 4596.
<https://stars.library.ucf.edu/etd/4596>

DECENTRALIZED POWER MANAGEMENT AND TRANSIENT CONTROL IN
HYBRID FUEL CELL ULTRA-CAPACITOR SYSTEM

by

OMID MADANI

B.S. Mechanical Engineering, Sharif University of Technology, 2009

M.S. Mechanical Engineering, University of Central Florida, 2011

A dissertation submitted in partial fulfillment of the requirements
for the degree of Doctor of Philosophy
in the Department of Mechanical and Aerospace Engineering
in the College of Engineering and Computer Science
at the University of Central Florida
Orlando, Florida

Fall Term
2014

Major Professor: Tuhin Das

© 2014 Omid Madani

ABSTRACT

Solid Oxide Fuel Cells (SOFCs) are considered suitable for alternative energy solutions due to advantages such as high efficiency, fuel flexibility, tolerance to impurities, and potential for combined cycle operations. One of the main operating constraints of SOFCs is fuel starvation, which can occur under fluctuating power demands. It leads to voltage loss and detrimental effects on cell integrity and longevity. In addition, reformer based SOFCs require sufficient steam for fuel reforming to avoid carbon deposition and catalyst degradation. Steam to carbon ratio ($STCR$) is an index indicating availability of the steam in the reformer. This work takes a holistic approach to address the aforementioned concerns in SOFCs, in an attempt to enhance applicability and adaptability of such systems. To this end, we revisit prior investigation on the *invariant properties* of SOFC systems, that led to prediction of fuel utilization U and $STCR$ in the absence of intrusive and expensive sensing. This work provides further insight into the reasons behind certain SOFC variables being invariant with respect to operating conditions. The work extends the idea of invariant properties to different fuel and reformer types.

In SOFCs, transient control is essential for U , especially if the fuel cell is to be operated in a dynamic load-following mode at high fuel utilization. In this research, we formulate a generalized abstraction of this transient control problem. We show that a multi-variable

systems approach can be adopted to address this issue in both time and frequency domains, which leads to input shaping. Simulations show the effectiveness of the approach through good disturbance rejection. The work further integrates the aforementioned transient control research with system level control design for SOFC systems hybridized with storage elements. As opposed to earlier works where centralized robust controllers were of interest, here, separate controllers for the fuel cell and storage have been the primary emphasis. Thus, the proposed approach acts as a bridge between existing centralized controls for single fuel cells to decentralized control for power networks consisting of multiple elements. As a first attempt, decentralized control is demonstrated in a SOFC ultra-capacitor hybrid system. The challenge of this approach lies in the absence of direct and explicit communication between individual controllers. The controllers are designed based on a simple, yet effective principle of conservation of energy. Simulations as well as experimental results are presented to demonstrate the validity of these designs.

To my Grandfather, my Parents, and Navid

ACKNOWLEDGMENTS

I would like to express my sincere appreciations to my advisor Dr. Tuhin Das, without whose kind consideration and wise guidance, I would not accomplish any of what I have achieved so far during the course of my graduate studies. Furthermore, I would like to thank my friend and colleague Amit Bhattacharjee who helped me vigorously, specifically for designing the experimental set-up and testing controllers. Moreover, I would like to appreciate and acknowledge the expert advice and helpful comments of Dr. Suhada Jayasuriya, the distinguished professor at Drexell University.

I would like to thank my parents who supported me throughout my life, specifically during my graduate studies. Thanks for never stopping encouraging me.

Finally, I would like to acknowledge the support provided by the NSF grant # 1158845 for conducting this research.

TABLE OF CONTENTS

LIST OF FIGURES	xii
LIST OF TABLES	xiv
CHAPTER 1 INTRODUCTION	1
1.1 Literature Review	1
1.2 Background	7
1.2.1 Reformer Model	8
1.2.2 SOFC Model	11
1.2.3 Fuel Utilization U	15
1.2.4 Addressing Transient Performance Using Invariant Property	16
1.3 Motivation	19
1.4 Contributions and Objectives	21

1.5	Dissertation Overview	21
CHAPTER 2 INVARIANT PROPERTIES IN FUEL CELL		24
2.1	Chapter Overview	24
2.2	Analysis of Steady-State Steam to Carbon Balance	25
2.2.1	Definition and Significance of STCR	25
2.2.2	General Steady-State Expression of STCB for SR-SOFC System	28
2.3	Control of Fuel Cell Using Invariant Property	31
2.3.1	Control Scheme Via $STCB_{ss}$	31
2.4	Performance Criteria for the Reformer and Fuel Cell Stack	33
2.4.1	STCR and STCB at the Stack	33
2.4.2	Performance Challenges	34
2.4.3	Healthy Performance Criteria	36
2.5	Chapter Summary	38

CHAPTER 3 TRANSIENT CONTROL IN MULTIVARIABLE SYSTEMS WITH AP- PLICATION IN SOFC	39
3.1 Chapter Overview	39
3.2 Output Controllability	40
3.2.1 What is Output Controllability?	40
3.2.2 Functional Output Controllability	43
3.2.3 Steady-State Output Controllability	45
3.2.4 Output Controllability in Nonlinear Systems	46
3.3 A Generalized Transient Control Problem	47
3.4 Problem Formulation for an LTI-MISO System	48
3.4.1 Complex Conjugate case	54
3.5 Problem Formulation in Frequency Domain	56
3.6 Generalized Transient Control Problem for LTI Systems	58
3.7 Transient Control in Linearized Fuel Cell Model	62

3.8	Chapter Summary	65
CHAPTER 4 DECENTRALIZED CONTROL FOR A FUEL CELL HYBRID POWER NETWORK		
4.1	Chapter Overview	66
4.2	Hybrid Network and Control Objectives	67
4.2.1	Control Objectives	68
4.3	Decentralized Control Using Conservation of Energy Principle	69
4.3.1	Approach	69
4.3.2	Implementation and Simulations	71
4.4	Decentralized Control Design	73
4.4.1	Design of K_1 using a Lower Bound on η_2 and $\bar{\eta}_2$	73
4.4.2	Dissipation Based Approach for Designing K_2	74
4.4.3	Voltage Regulation Based Approach for K_2	79
4.5	Experimental Results	82

4.5.1	Dissipation Based Approach	84
4.5.2	Voltage regulation approach	85
4.6	OBSERVATIONS	86
4.6.1	Overall System Loss Trends	86
4.6.2	Comparison between Centralized and Decentralized Strategies	87
4.7	Area Matching Using Dynamic Response of System	88
4.7.1	Second Order Under-damped Systems	89
4.8	Chapter Summary	91
CHAPTER 5 CONCLUSIONS		92
LIST OF REFERENCES		95

LIST OF FIGURES

Figure 1.1	Schematic Diagram of SOFC System [1]	7
Figure 1.2	Schematic diagram of tubular steam reformer [1]	9
Figure 1.3	Schematic diagram of tubular SOFC [1]	12
Figure 1.4	Open-loop Response to Transient Current Demand [2]	17
Figure 1.5	Transient Control of U through Current Regulation	18
Figure 1.6	Simulations showing Transient Control of U , (from [3])	19
Figure 2.1	Simulation Results for STCB-Based Current Regulation Approach	32
Figure 2.2	Comparison of STCR and STCB for Both Reformer and Stack	34
Figure 2.3	Simulation Results for U -Based Current Regulation Approach with Lagged Current	37
Figure 3.1	Simulation Showing Isolation Of y From Exogenous Input u_1 During Transients. 52	
Figure 3.2	Comparison Of Transient Response For Three Different C Matrices.	53
Figure 3.3	Isolation Of y From Exogenous Input u_1 using Eq.(3.44)	61
Figure 4.1	Schematic of Hybrid Fuel Cell System with Decentralized Control	67

Figure 4.2	Conservation of Energy Approach	69
Figure 4.3	Energy Conservation based Control with Known η_2 and $\bar{\eta}_2$	72
Figure 4.4	Energy Conservation with a Conservative Estimate of η_2 and $\bar{\eta}_2$	73
Figure 4.5	Dissipation Circuit Schematic	74
Figure 4.6	System response with a P controller for dissipation	75
Figure 4.7	System response with a PI controller for dissipation	77
Figure 4.8	Simulations with Voltage Modulation and Efficiency Estimation	81
Figure 4.9	Experimental Test Stand	83
Figure 4.10	Experimental Results for Dissipation Based Approach	84
Figure 4.11	Experimental Results for Voltage Regulation Based Approach-Powers	85
Figure 4.12	Power Loss Trends with Voltage Regulation and Dissipation Approaches	87

LIST OF TABLES

Table 4.1	Equipment specifications	82
-----------	------------------------------------	----

CHAPTER 1

INTRODUCTION

1.1 Literature Review

Solid Oxide Fuel Cells (SOFC) are high temperature ($800^{\circ} - 1000^{\circ}\text{C}$) energy conversion devices that allow internal reforming and sustain on-board fuel reforming by promoting rapid reaction kinetics with non-precious metals. SOFCs produce high quality by-product heat for co-generation or for use in a bottoming cycle [4, 5]. Moreover, they offer numerous benefits such as working with a wide range of fuels, immunity to pollution and impurities in fuels, relatively high efficiency, and potential to replace large-scale power plants as a nominee for small-scale power generation [6]. However, Long response time and poor load following capability seems to be the most bothersome obstacles to restrict extensive application of SOFCs [7]. These issues are mostly caused by fuel starvation which could occur while SOFC is subjected to a sudden change in power demand (see details in [8] and references therein).

Fuel starvation is mainly caused by the lags introduced by the fuel supply system and the reformer [9, 10, 11, 12, 13]. The phenomenon adversely affects cell durability through anode oxidation [13] and reversal of cell potential, leading to catalyst corrosion [14]. To address these issues, authors in [9] develop various reference governors by using a model predictive approach. Similarly, researchers in [15] address the same problems by using a linear

compensator to modify the target fuel flow. While both methods reduce the susceptibility to fuel starvation, they are both model dependent. Furthermore, both methods have an adverse effect on the load following capability of the SOFC. To improve load following, authors of [16] develop a control method based on constant utilization operation, as well as a control structure to keep the combustor temperature within acceptable range.

Constant fuel utilization (U) is the primary mode of operation of SOFCs [17, 18, 19, 9]. Hydrogen starvation in SOFCs can be prevented by limiting the fluctuations in fuel utilization from a set-point value under transient power demands. The target fuel utilization is typically chosen between 80% to 90% for high efficiency [20, 21, 22, 23]. Other operating modes include constant fuel supply operation [18] and constant voltage operation [24]. In the constant fuel utilization mode, the fuel flow is varied to maintain U at a set-point ($\approx 85\%$). This approach is particularly favored since U is a direct indicator of hydrogen starvation. One method to maintain constant U is to vary fuel flow rate assuming U is measured [25, 17]. While this is acceptable in simulation based studies, in practice measuring U requires several species-specific concentration sensors that are avoided due to cost and reliability considerations [26]. Observer designs are possible; however, they can be computationally intensive, and rely on accurate mathematical models [27, 28, 29]. Another method is to use an analytical equation relating U , fuel flow, and current draw in steady-state. The equation is used to manipulate fuel flow based on current demand. Prior work done in [3] proposes a current regulation method to attenuate the aforementioned fluctuations in utilization. More details of this

method and discussions on the importance of fuel utilization in SOFC systems can be found in [1, 3, 8] and references therein.

It is noteworthy that while works on transient control in SOFCs is limited in the literature, a significant proportion of research done on the transient control of fuel cells is devoted to Polymer Electrolyte Membrane (PEM) fuel cells where oxygen starvation poses similar issues [30, 31, 32, 33, 12]. Existing methods of mitigation include use of reference governors [32, 34], or Model Predictive Control (MPC) [35, 12]. Moreover, Authors in [31] indicated that with a feedback control of the air-compressor-motor voltage, the oxygen level could be maintained in the cathode. Alternatively, Espiari et al. [36], has investigated the effect of temperature variations during transients within different fuel cell parts. Furthermore, in [33], authors have employed a fuel regulation method to limit the hydrogen fed into the cell through changing the internal resistance of the membrane to control the power output of the PEMFC.

Even though oxygen starvation in PEMs and hydrogen starvation in SOFCs have some similarities such as excessive voltage drop, the two fuel cells are inherently different mandating different approaches for addressing these starvation phenomena. Most importantly, the fuel supply to SOFC anode is a gas mixture containing several species with varying and unknown concentrations due to fuel flexibility and internal reforming reactions. In contrast, in PEMs the fuel is pure hydrogen only, and air supply has a fixed and known amount of oxygen. This is an important reason why model-based control of SOFCs poses a major challenge but is more tractable for PEMs.

On the other hand, some researchers have focused on the modeling of SOFC from dynamics and control's perspective. To name a few, Das et al. [1] has proposed a comprehensive control-oriented model for SOFC system. A similar work was done by [13] where a two-dimensional dynamic model was created for an actual SOFC system in which the effect of several parameters including fuel utilization and fuel flow delays were investigated. A comprehensive review of solid oxide fuel cell Dynamic models can be found in [37, 38, 39] and references therein.

Simultaneously preventing hydrogen starvation and improving load following can be achieved by hybridizing the SOFC with an energy storage device such as battery or capacitor [40, 41]. Authors in [42] have utilized the idea of hybridizing the PEMFC with super-capacitors for automotive applications. Similarly, in [43], the concept of hybrid power sources is introduced in which PEMFC is nominated as the main source and batteries or super-capacitors as auxiliary power source. Furthermore, Payman in [44] has used a flatness-based nonlinear control approach to control a hybrid system of fuel cell and super-capacitor bank. In this regard, authors in [45] outlined an adaptive controller for active power sharing in the hybrid system of fuel cell and batteries. Their control strategy is based on adjusting the setpoint of the output current of the fuel cell according to the voltage of the battery. Similar works can be found at [46, 47, 48].

Despite all advantages, fairly fewer researchers have worked on hybridization of SOFC to improve load following capabilities. In [49], a novel control scheme for improving the operation of SOFC/battery hybrid was introduced which included a supervisory controller

which seizes all operation modes. Another case in point is the control strategies developed by Allag et al. [3] which included a Lyapunov-based nonlinear controller and a standard H_∞ robust controller. Additionally, authors developed an adaptive controller for a hybrid SOFC system in [50]. A supervisory controller for a SOFC ultra-capacitor hybrid, based on fuzzy logic was also designed in [51].

The works mentioned above can be categorized as centralized power management schemes where sensed information is directed toward a central processor that commands all components of the system. While centralized control is easier to develop, practical issues can arise in scaling-up to bigger networks. When posed as an optimization problem, high dimensions is an issue for current micro-controllers as the number of energy resources in the network increases [34]. Also, in case the central controller encounters any malfunction, the entire network is influenced. Furthermore, if the network topology is subject to change, a central controller may need to be reprogrammed. Hence, the idea of decentralized power management is worth exploring, where information processing takes place in component-level controllers that have little or no communication between each other. While the idea of decentralized control of SOFC appears in [52], it interprets decoupled PID loops within the SOFC controller as decentralized control. In contrast, our work considers decentralization for power management in a network consisting of the SOFC and an ultra-capacitor.

In recent years, there has been growing interest in distributed control in the context of large scale networked systems. For such systems, the constraints posed by implementation, cost and reliability should be given their due importance. The size and the complexity of

such systems necessitate decentralized control. An elaborate description of such systems can be found in [53]. The main difficulties are dimensionality, information structure constraints, uncertainty, and delay. In this regard, decentralized stabilization of interconnected dynamical systems appears in [54, 55]. Decentralized control with specific emphasis on power grids appears in [56, 57], where the authors address robust stability of large-scale power systems. On the other hand, operation of such large scale systems is also expected to be fault tolerant and reliable. To this end, the issue of cascaded tripping in power networks is addressed via a decentralized architecture in [58]. In [59], a novel decentralized fault tolerant control structure was developed using droop control. Also, a multi-agent based decentralized control using a novel optimization framework was proposed in [60] to mitigate cascaded failures in power system.

SOFC is deemed a fitting candidate for distributed generation in grids due to its many advantages [61, 62]. In this regard, authors in [63] attempt to improve grid-application of SOFCs through control design and suitable power conditioning systems. In addition, active power filters are proposed in [41] to improve the power quality as well as to mitigate any adverse grid impact of stationary SOFC systems. With the over-arching goal of developing a decentralized control paradigm for SOFC systems in a power network, we attempt to formulate a simpler problem as a first step. We design decentralized control for a hybrid SOFC ultra-capacitor system. Two separate controllers are proposed, one for the SOFC and the other for the ultra-capacitor, that have no communication between each other. The former operates the fuel cell in a load-following mode, while attenuating transient fluctuations

in the fuel utilization. The latter allows the ultra-capacitor to be used as an energy buffer. The novelty of this work lies in the energy conservation based mechanism that is incorporated in the SOFC controller. It anticipates the deficit or excess energy of the capacitor based on the SOFC's transient response history, without communicating with the ultra-capacitor. The capacitor control, in turn, imparts robustness to the performance of the decentralized system by either dissipating excess energy or regulating the load voltage. Together, synergistic power management is realized.

1.2 Background

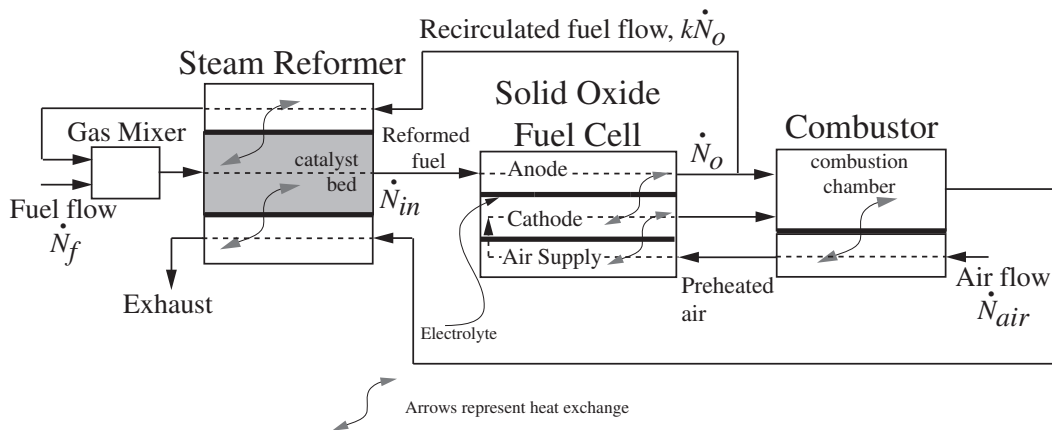


Figure 1.1: Schematic Diagram of SOFC System [1]

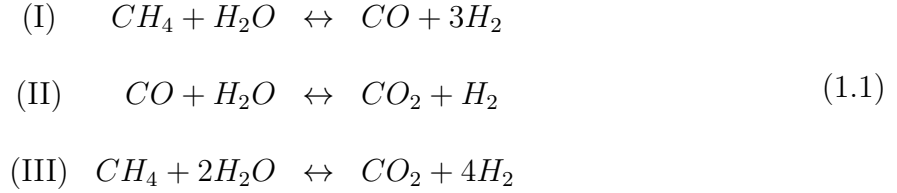
In this work, we consider a tubular SOFC which is essentially constructed by three major parts i.e. the steam reformer, the fuel cell stack and the combustor. In the model presented here, primary fuel is chosen to be Methane with a molar flow rate of \dot{N}_f . However, the methodology and approach used here can be employed for other fuels and system configurations. The system is illustrated in Fig.1.1. The reformer produces a hydrogen-rich

gas which is supplied to the anode of the fuel cell. Electrochemical reactions occurring at the anode due to current draw results in a steam-rich gas mixture at its exit. A known fraction k of the anode exhaust is recirculated through the reformer into a mixing chamber where fuel is added. The mixing of the two fluid streams and pressurization is achieved in the gas mixer using an ejector or a recirculating fuel pump [64]. The steam reforming process occurring in the reformer catalyst bed is an endothermic process. The energy required to sustain the process is supplied from two sources, namely, the combustor exhaust that is passed through the reformer, and the aforementioned recirculated anode flow, as shown in Fig.1.1. The remaining anode exhaust is mixed with the cathode exhaust in the combustion chamber. The combustor also serves to preheat the cathode air which has a molar flow rate of \dot{N}_{air} . The tubular construction of each cell causes the air to first enter the cell through the air supply tube and then reverse its direction to enter the cathode chamber.

1.2.1 Reformer Model

In this section, we first, review the model we have used for the reformer and stack from the electrochemical standpoint briefly. More details about this model can be found in [1]. For steam reforming of methane we consider a packed-bed tubular reformer with nickel-alumina catalyst [65]. A schematic diagram of the steam reformer is shown in Fig.1.2. The exhaust, reformate and recirculated flows are modeled using gas control volumes and the catalyst bed is modeled as a solid volume. The details of the heat transfer characteristics of the system can be found in [13] and is not repeated here. Instead, we emphasize on the

reformer reaction kinetics and the mass transfer phenomena in light of the analyses presented in the following sections. As discussed earlier, the three main reactions that simultaneously occur during steam reforming of methane are, [25], [66]:



From Fig.1.1, the mass balance equations for CH_4 , CO , CO_2 , H_2 and H_2O can be written as follows:

$$\begin{aligned}
 N_r \dot{\mathcal{X}}_{1,r} &= k \dot{N}_o \mathcal{X}_{1,a} - \dot{N}_{in} \mathcal{X}_{1,r} + \mathcal{R}_{1,r} + \dot{N}_f \\
 N_r \dot{\mathcal{X}}_{2,r} &= k \dot{N}_o \mathcal{X}_{2,a} - \dot{N}_{in} \mathcal{X}_{2,r} + \mathcal{R}_{2,r} \\
 N_r \dot{\mathcal{X}}_{3,r} &= k \dot{N}_o \mathcal{X}_{3,a} - \dot{N}_{in} \mathcal{X}_{3,r} + \mathcal{R}_{3,r} \\
 N_r \dot{\mathcal{X}}_{4,r} &= k \dot{N}_o \mathcal{X}_{4,a} - \dot{N}_{in} \mathcal{X}_{4,r} + \mathcal{R}_{4,r} \\
 N_r \dot{\mathcal{X}}_{5,r} &= k \dot{N}_o \mathcal{X}_{5,a} - \dot{N}_{in} \mathcal{X}_{5,r} + \mathcal{R}_{5,r}
 \end{aligned}
 \tag{1.2}$$

where $N_r = P_r V_r / R_u T_r$.

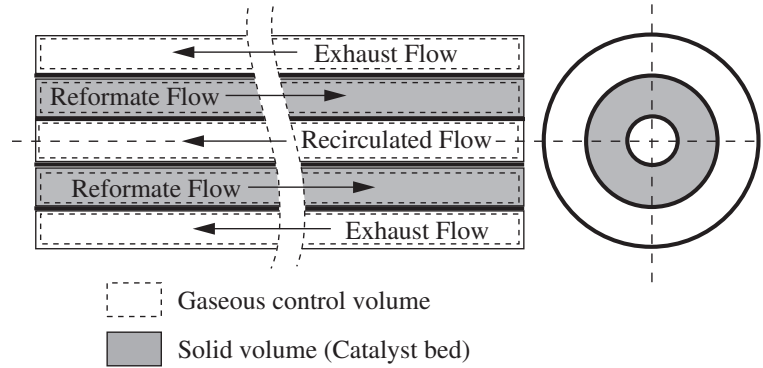


Figure 1.2: Schematic diagram of tubular steam reformer [1]

Note that the reformer inlet and exit flows shown in Fig.1.1 do not contain O_2 and N_2 . Hence $\mathcal{X}_{6,r} = \mathcal{X}_{7,r} = 0$. From Eq.(1.1), we express $\mathcal{R}_{j,r}$, $j = 1, 2, \dots, 5$, in terms of the reaction rates r_I , r_{II} and r_{III} as follows

$$\mathbf{R}_r = \mathbf{G} \mathbf{r}, \quad \mathbf{R}_r = \begin{bmatrix} \mathcal{R}_{1,r} \\ \mathcal{R}_{2,r} \\ \mathcal{R}_{3,r} \\ \mathcal{R}_{4,r} \\ \mathcal{R}_{5,r} \end{bmatrix}, \quad \mathbf{r} = \begin{bmatrix} r_I \\ r_{II} \\ r_{III} \end{bmatrix}, \quad \mathbf{G} = \begin{bmatrix} -1 & 0 & -1 \\ 1 & -1 & 0 \\ 0 & 1 & 1 \\ 3 & 1 & 4 \\ -1 & -1 & -2 \end{bmatrix} \quad (1.3)$$

Since \mathbf{G} has a rank of 2, therefore there are only two independent reaction rates among $\mathcal{R}_{j,r}$, $j = 1, 2, \dots, 5$. Considering the rate of formation of CH_4 and CO in the reformer to be independent, we can write

$$\begin{aligned} \mathcal{R}_{3,r} &= -\mathcal{R}_{1,r} - \mathcal{R}_{2,r} \\ \mathcal{R}_{4,r} &= -4\mathcal{R}_{1,r} - \mathcal{R}_{2,r} \\ \mathcal{R}_{5,r} &= 2\mathcal{R}_{1,r} + \mathcal{R}_{2,r} \end{aligned} \quad (1.4)$$

and rewrite Eq.(1.2) as follows:

$$\begin{aligned}
N_r \dot{\mathcal{X}}_{1,r} &= k\dot{N}_o \mathcal{X}_{1,a} - \dot{N}_{in} \mathcal{X}_{1,r} + \mathcal{R}_{1,r} + \dot{N}_f \\
N_r \dot{\mathcal{X}}_{2,r} &= k\dot{N}_o \mathcal{X}_{2,a} - \dot{N}_{in} \mathcal{X}_{2,r} + \mathcal{R}_{2,r} \\
N_r \dot{\mathcal{X}}_{3,r} &= k\dot{N}_o \mathcal{X}_{3,a} - \dot{N}_{in} \mathcal{X}_{3,r} - \mathcal{R}_{1,r} - \mathcal{R}_{2,r} \\
N_r \dot{\mathcal{X}}_{4,r} &= k\dot{N}_o \mathcal{X}_{4,a} - \dot{N}_{in} \mathcal{X}_{4,r} - 4\mathcal{R}_{1,r} - \mathcal{R}_{2,r} \\
N_r \dot{\mathcal{X}}_{5,r} &= k\dot{N}_o \mathcal{X}_{5,a} - \dot{N}_{in} \mathcal{X}_{5,r} + 2\mathcal{R}_{1,r} + \mathcal{R}_{2,r}
\end{aligned} \tag{1.5}$$

From Eq.(1.5) we deduce

$$\dot{N}_{in} = k\dot{N}_o + \dot{N}_f + \sum_{j=1}^7 \mathcal{R}_{j,r} \quad \Rightarrow \quad \dot{N}_{in} = k\dot{N}_o + \dot{N}_f - 2\mathcal{R}_{1,r} \tag{1.6}$$

The models of internal reforming reaction rates r_I , r_{II} and r_{III} can be found in [1].

1.2.2 SOFC Model

We assume our system to be comprised of \mathcal{N}_{cell} tubular Solid Oxide Fuel Cells, connected in series. A schematic diagram of an individual cell is shown in Fig.1.3. The anode, cathode and feed air flows are modeled using gas control volumes. The air feed tube and the electrolyte are modeled as solid volumes. Details of the heat transfer model and voltage computations can be found in [13] and is not repeated here. As in the previous section, we emphasize on the fuel cell chemical kinetics and mass transfer phenomena.

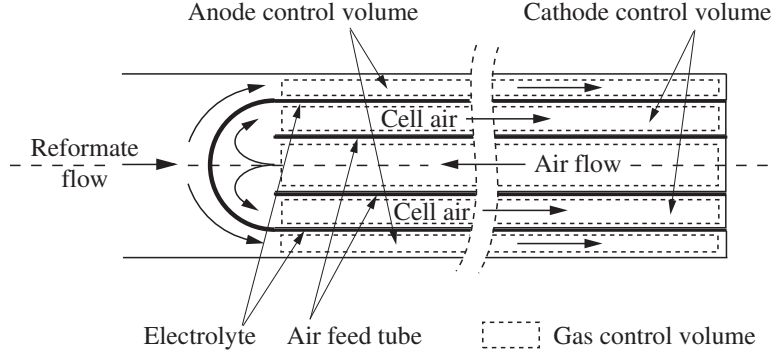
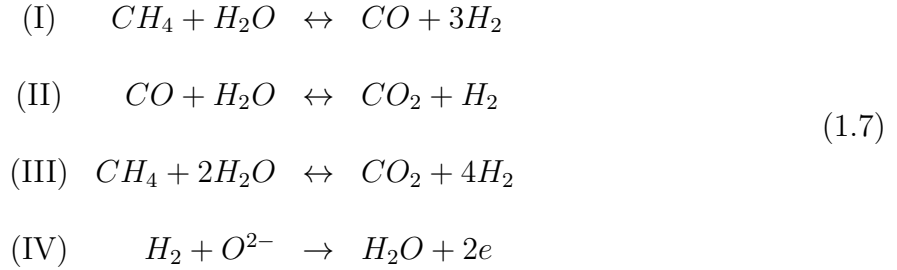


Figure 1.3: Schematic diagram of tubular SOFC [1]

Anode control volume: The following chemical and electro-chemical reactions occur simultaneously in the anode control volume:



Steam reforming, represented by reactions I, II and III, occur in the anode due to high temperatures and the presence of nickel catalyst. The primary electrochemical process is steam generation from H_2 , described by reaction IV. Simultaneous electrochemical conversion of CO to CO_2 in the anode is also possible. However, this electro-chemical reaction is ignored since its reaction rate is much slower in presence of reactions II and IV, as indicated in [67] and references therein.

From Fig.1.1, the mass balance equations for CH_4 , CO , CO_2 , H_2 and H_2O can be written as

$$\begin{aligned}
N_a \dot{\mathcal{X}}_{1,a} &= -\dot{N}_o \mathcal{X}_{1,a} + \dot{N}_{in} \mathcal{X}_{1,r} + \mathcal{R}_{1,a} \\
N_a \dot{\mathcal{X}}_{2,a} &= -\dot{N}_o \mathcal{X}_{2,a} + \dot{N}_{in} \mathcal{X}_{2,r} + \mathcal{R}_{2,a} \\
N_a \dot{\mathcal{X}}_{3,a} &= -\dot{N}_o \mathcal{X}_{3,a} + \dot{N}_{in} \mathcal{X}_{3,r} + \mathcal{R}_{3,a} \\
N_a \dot{\mathcal{X}}_{4,a} &= -\dot{N}_o \mathcal{X}_{4,a} + \dot{N}_{in} \mathcal{X}_{4,r} + \mathcal{R}_{4,a} - r_e \\
N_a \dot{\mathcal{X}}_{5,a} &= -\dot{N}_o \mathcal{X}_{5,a} + \dot{N}_{in} \mathcal{X}_{5,r} + \mathcal{R}_{5,a} + r_e
\end{aligned} \tag{1.8}$$

where $N_a = P_a V_a / R_u T_a$ and r_e is the rate of electrochemical reaction given by

$$r_e = \frac{i \mathcal{N}_{cell}}{nF} \tag{1.9}$$

Since current i can be measured, the rate of electrochemical reaction r_e is considered known. As with the reformate control volume, the anode inlet and exit flows do not contain O_2 and N_2 . Therefore, $\mathcal{X}_{6,a} = \mathcal{X}_{7,a} = 0$. From Eq.(1.7), we express $\mathcal{R}_{j,a}$, $j = 1, 2, \dots, 5$, in terms of the reaction rates r_I , r_{II} and r_{III} as follows

$$\mathbf{R}_a = \mathbf{G} \mathbf{r} + r_e [0 \ 0 \ 0 \ -1 \ 1]^T \tag{1.10}$$

where $\mathbf{R}_a = [\mathcal{R}_{1,a} \ \mathcal{R}_{2,a} \ \mathcal{R}_{3,a} \ \mathcal{R}_{4,a} \ \mathcal{R}_{5,a}]^T$, and \mathbf{G} and \mathbf{r} are given in Eq.(1.3). Since \mathbf{G} has a rank of 2 and r_e is known, therefore there are only two independent reaction rates among

$\mathcal{R}_{j,a}$, $j = 1, 2, \dots, 5$. Considering $\mathcal{R}_{1,a}$ and $\mathcal{R}_{2,a}$ to be independent, we can write

$$\begin{aligned}
\mathcal{R}_{3,a} &= -\mathcal{R}_{1,a} - \mathcal{R}_{2,a}, \\
\mathcal{R}_{4,a} &= -4\mathcal{R}_{1,a} - \mathcal{R}_{2,a} - r_e, \\
\mathcal{R}_{5,a} &= 2\mathcal{R}_{1,a} + \mathcal{R}_{2,a} + r_e
\end{aligned} \tag{1.11}$$

and rewrite Eq.(1.8) as

$$\begin{aligned}
N_a \dot{\mathcal{X}}_{1,a} &= -\dot{N}_o \mathcal{X}_{1,a} + \dot{N}_{in} \mathcal{X}_{1,r} + \mathcal{R}_{1,a} \\
N_a \dot{\mathcal{X}}_{2,a} &= -\dot{N}_o \mathcal{X}_{2,a} + \dot{N}_{in} \mathcal{X}_{2,r} + \mathcal{R}_{2,a} \\
N_a \dot{\mathcal{X}}_{3,a} &= -\dot{N}_o \mathcal{X}_{3,a} + \dot{N}_{in} \mathcal{X}_{3,r} - \mathcal{R}_{1,a} - \mathcal{R}_{2,a} \\
N_a \dot{\mathcal{X}}_{4,a} &= -\dot{N}_o \mathcal{X}_{4,a} + \dot{N}_{in} \mathcal{X}_{4,r} - 4\mathcal{R}_{1,a} - \mathcal{R}_{2,a} - r_e \\
N_a \dot{\mathcal{X}}_{5,a} &= -\dot{N}_o \mathcal{X}_{5,a} + \dot{N}_{in} \mathcal{X}_{5,r} + 2\mathcal{R}_{1,a} + \mathcal{R}_{2,a} + r_e
\end{aligned} \tag{1.12}$$

From Eq.(1.12) we deduce that

$$\dot{N}_o = \dot{N}_{in} + \sum_{j=1}^7 \mathcal{R}_{j,a} \Rightarrow \dot{N}_o = \dot{N}_{in} - 2\mathcal{R}_{1,a} \tag{1.13}$$

Cathode control volume: Ionization of O_2 in the cathode control volume occurs through the reaction



with the reaction rate as given in Eq.(1.9). Considering the mole fractions of N_2 and O_2 in air to be 0.79 and 0.21 respectively, the mass balance equations of the cathode control volume can be written from Eqs.(1.9) and (1.14) as follows:

$$\begin{aligned}
N_c \dot{\mathcal{X}}_{6,c} &= 0.79 \dot{N}_{air} - \left(\dot{N}_{air} - 0.5r_e \right) \mathcal{X}_{6,c} \\
N_c \dot{\mathcal{X}}_{7,c} &= 0.21 \dot{N}_{air} - \left(\dot{N}_{air} - 0.5r_e \right) \mathcal{X}_{7,c} - 0.5r_e \\
\mathcal{X}_{j,c} &= 0, \quad j = 1, 2, \dots, 5
\end{aligned} \tag{1.15}$$

More details about the other features of this model can be found in [1, 3].

1.2.3 Fuel Utilization U

Fuel utilization U is mathematically defined as, [13, 21, 20]:

$$U \triangleq 1 - \frac{\dot{N}_o (4\mathcal{X}_{1,a} + \mathcal{X}_{2,a} + \mathcal{X}_{4,a})}{\dot{N}_{in} (4\mathcal{X}_{1,r} + \mathcal{X}_{2,r} + \mathcal{X}_{4,r})} \tag{1.16}$$

where, $\mathcal{X}_{1,a}$, $\mathcal{X}_{2,a}$, $\mathcal{X}_{4,a}$ and $\mathcal{X}_{1,r}$, $\mathcal{X}_{2,r}$, $\mathcal{X}_{4,r}$ are the molar concentrations of CH_4 , CO and H_2 in the anode and the reformer respectively and \dot{N}_o and \dot{N}_{in} are shown in Fig.1.1. Eq.(1.16) is based on the observation that a CH_4 and a CO molecule can yield at most four molecules and one molecule of H_2 respectively, as indicated by reactions I, II and III in Eq.(1.7).

Having done some algebra [3, 2], the steady-state utilization U_{ss} is obtained as [3]

$$U_{ss} = \frac{1 - k}{\left(4nF\dot{N}_f / i_{fc} \mathcal{N}_{cell} \right) - k} \tag{1.17}$$

Note that Eq.(1.17) is independent of the reaction rates $\mathcal{R}_{1,r}$, $\mathcal{R}_{2,r}$, $\mathcal{R}_{1,a}$, $\mathcal{R}_{2,a}$ and the flow rates \dot{N}_{in} , \dot{N}_o . Equation (1.17) is valid in steady-state and is invariant with respect to variations in operating temperature, operating pressure, mass of reforming catalyst, air flow rate and operating Steam-to-Carbon ratio [1]). Thus, Eq.(1.17) represents *an invariant relationship* between steady-state fuel utilization U_{ss} , fuel cell current i_{fc} , and fuel flow rate \dot{N}_f . Given a target U_{ss} , it can be used to determine \dot{N}_f if i_{fc} is known and vice-versa [3].

The invariant property can serve as an open-loop control for constant utilization operation. However, it is a steady-state property and hydrogen starvation must be prevented even during transient operation. Typically, U must be around an optimal value ($\approx 85\%$) within narrow limits ($\pm 5\%$) even under significant power fluctuations. The limitation of using the invariant property alone in an open-loop control is demonstrated in simulations presented in the following sections where instantaneous changes in power demand are applied through step-changes in current demand $i_{fc,d}$.

1.2.4 Addressing Transient Performance Using Invariant Property

To demonstrate the SOFC's vulnerability to current draw without proper control, a simulation result is depicted in Fig. 1.4. Here, we have considered a tubular SOFC model, with 50 cells connected in series, each cell having a length of 251cm, fuel flow of 7×10^{-4} moles/s and a current draw of 10A for $t < 150$ s. Using these values, U will be approximately 85%. It is shown that fuel cell is not even able to endure a 1A increase in current load due to hydrogen starvation. This result shows the importance of a proper con-

trol as fuel cell performance can be easily disturbed facing small perturbations [2].

To address this issue, we refer to [3] in which this transient issue was discussed in details; However, to demonstrate the motivation for this work, we review how this problem was solved in [3] briefly.

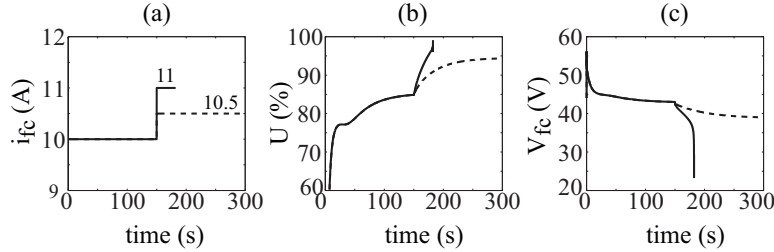


Figure 1.4: Open-loop Response to Transient Current Demand [2]

For a desired steady-state utilization U_{ss} , and a given demanded fuel cell current $i_{fc,d}$, a fuel flow demand $\dot{N}_{f,d}$ can be calculated from Eq.(1.17), given by,

$$\dot{N}_{f,d} = \frac{i_{fc,d} \mathcal{N}_{cell}}{4nFU_{ss}} [1 - (1 - U_{ss})k] \quad (1.18)$$

Note that as is shown in Fig.1.1, the Fuel Supply System (FSS) provides fuel flow \dot{N}_f in response to the demand $\dot{N}_{f,d}$, and Eq.(1.18) ensures that at steady-state $U = U_{ss}$. However, during transience, due to the lag associated with the FSS, $\dot{N}_{f,d} \neq \dot{N}_f$. This results in fluctuations in U around U_{ss} . Large changes in $i_{fc,d}$ can result in hydrogen starvation ($U \rightarrow 100\%$). This is illustrated through simulation results shown in Fig. 1.6(a1-d1). To address this issue, we propose the current regulation method by reversing Eq.(1.18) to calculate the

regulated current based on the actual fuel flow, \dot{N}_f , given by

$$i_{fc} = \frac{4nFU_{ss}\dot{N}_f}{\mathcal{N}_{cell}} \frac{1}{[1 - (1 - U_{ss})k]} \quad (1.19)$$

This current regulation approach as well as lags associated with fuel flow are illustrated in Fig.1.5 with the switch position labeled CR.

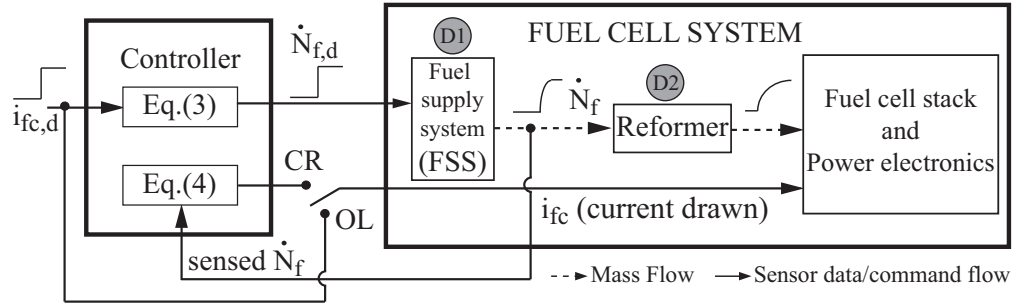


Figure 1.5: Transient Control of U through Current Regulation

In comparison, the open-loop (i.e. unregulated current) approach corresponds to the switch position OL. The proposed current regulation method has similarities with existing model-based approaches for PEMFC and SOFC systems using current filter or load governor, [30, 32, 29]. Note that CR assumes no knowledge of the dynamic characteristics of the FSS. Improvement in transient response of U in CR over OL is depicted in Fig.1.6. Details of the simulations and the model can be found in [3, 1]. As shown, CR allows significantly greater fluctuations in load compared to OL, Figs.1.6(a1) and (a2), before the onset of fuel starvation, Figs.1.6(c1) and (c2).

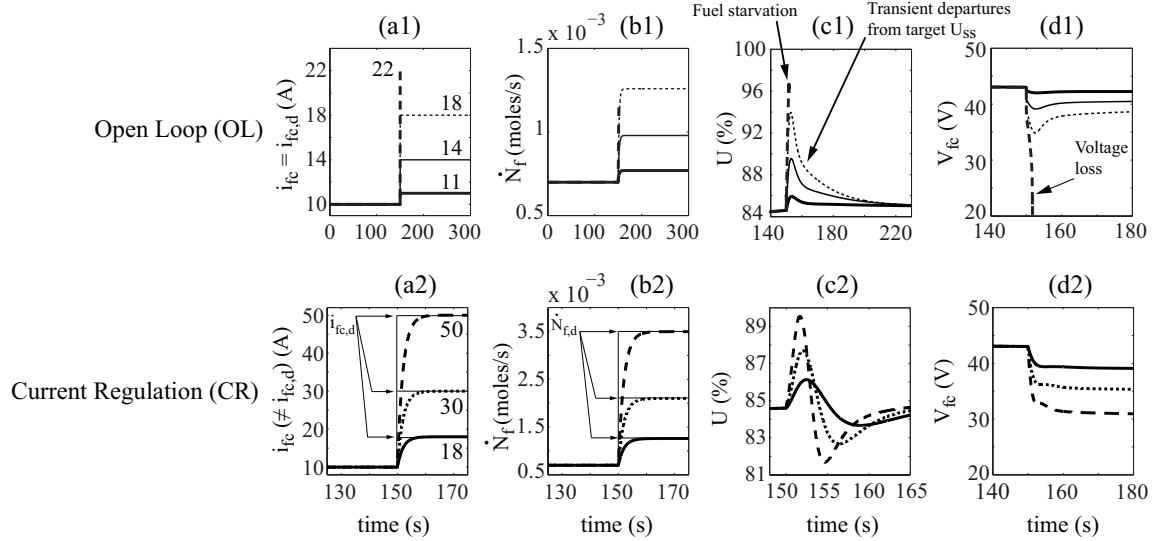


Figure 1.6: Simulations showing Transient Control of U , (from [3])

However, this approach also creates a disparity between $i_{f,c,d}$ and $i_{f,c}$ during transients (see Fig.1.6(a2)). This implies that while current regulation protects the fuel cell from fuel starvation due to power fluctuations, it results in a disparity between the demanded and delivered power during transients. This disparity amounts to deficient load-following, that is addressed by hybridizing the fuel cell with an ultra-capacitor.

1.3 Motivation

In many cases, it is needed to design the control inputs such that the output is independent of one of the exogenous inputs. Specifically, this is the case for SOFCs in which the actual fuel flow rate is governed by power demand, which is an exogenous input. Therefore, we want to design the control input, namely the current draw from the fuel cell, in a way that U undergoes minimum transient fluctuations in the presence of load transients.

One could argue that this could be done by sensing the molar fractions of different species in different locations inside the cell; In other words, measuring U at any instant and then designing the controls accordingly. Granted this option is possible, it requires too much intrinsic sensing within the cell which can be very expensive as well as difficult to implement. Furthermore, estimating U is another possibility through which a control scheme can be developed. Yet, that requires a comprehensive model, and state estimator performance would be largely governed by the accuracy of the plant model, which is very approximate in this case. Hence, the challenge and also the novelty of this work is to control the transients of the output while no instantaneous information of the system is provided but the steady state information.

As is shown in Fig.1.6, the transient response of the system is within an acceptable range even though not much information was provided except the steady state equation of the fuel utilization (output). This observation prompted us to think whether this method could be generalized to other cases where the transient control is needed for plants for which not much information is provided. Further discussion and details on this problem can be found in chapter 3.

On the other hand, when it comes to SOFC hybrid networks, the concept of decentralized control is fairly novel in the domain of power grids and control systems. The novelty of this work lies within the simplicity and practicality of the energy conservation method which is the essence of the developed controllers here. Moreover, lack of any communication between controllers enables the control scheme to be scaled up to a much broader network

with multiple elements.

1.4 Contributions and Objectives

The objectives and contributions of this work can be summarized as follows:

1. Propose a novel method for perfect transient control for a multivariable system for which sensing or estimation is not available.
2. Prove the invariance of a general parameter under steady-state condition whose monitoring is vital to the health of reformer.
3. Develop a decentralized control scheme for hybrid power network consisting a single SOFC and an Ultra-capacitor.
4. Develop separate controllers for FC side an UC side without any direct communication.
5. Verify the developed controllers in simulations.
6. Verify the developed controllers on an experimental test-stand.

1.5 Dissertation Overview

In this Dissertation, after discussing some preliminaries and reviewing the existing works related to the subject in Chapter 1, in Chapter 2, we introduce *STCR* and *STCB* that are highly important to be monitored to guarantee a safe operation in the reformer.

Then, we prove some facts about those parameters and outline their importance in the safe operation of the SOFC System. Consequently, in Chapter 3, we initially present a review of output controllability criteria which potentially could be related to the problem which we have formulated and discussed later on in this chapter. Then, we focus on the transient control of U as a theoretical problem. We show through both analysis and simulations that a generalized abstraction of the transient control problem in SOFCs is possible. The main idea is that in a multi-input single output system, under certain conditions, it is possible to achieve complete isolation of the output from exogenous input(s) by shaping control inputs, even if the plant is largely unknown or partially known and the output variable itself is not measurable. Such a generalized problem can be posed for non-linear time-varying systems and also for linear time invariant systems. For the latter category of systems, we derive analytical conditions under which the problem is solvable. We also show how these conditions are somewhat satisfied by the fuel cell system, and consequently yield acceptable transient control of U even though the SOFC system is non-linear and time-varying. On the other hand, a brief review of decentralized control and the motivation of this work will be presented in Chapter 4. Then, it will be followed by a concise description of the fuel cell model and its hybridization with ultra-capacitor is presented. Then, the theory and concept of decentralized approach which we have employed will be explained. Next, separate local controllers for each fuel side and ultra-capacitor side will be introduced. A conservation of energy based controller for fuel cell side and two separate controllers for the ultra-capacitor side will be outlined. The first FC side controller leads into gradual over-charging of the

ultra-capacitor which mandates energy dissipation to adjust the UC state of charge. On the other hand, out of two proposed controllers for UC side, one uses a PWM circuit to dissipate extra energy, and the other uses voltage modulation to tailor the capacitor's stored energy. In the latter approach, the FC observes the manipulated voltage and interprets that information to gradually decrease uncertainties over time. Following to the theoretical discussion, the experimental results are presented as well to verify the proposed controllers' performance.

Finally, the document is concluded with a summary of what has been done throughout the entire research we have conducted in chapter 5. Thereafter, the references are provided.

CHAPTER 2 INVARIANT PROPERTIES IN FUEL CELL

1

2.1 Chapter Overview

In order to avoid carbon deposition and catalyst degradation, reformer needs to access sufficient steam to carry on the reforming reaction. Steam to carbon ratio ($STCR$) is an index indicating availability of the steam in the reformer. In this chapter, we first define a new variable called steam to carbon balance ($STCB$) based on $STCR$, and show that for steam reformer based SOFCs which utilize Methane as the main fuel, the steady-state $STCB$ is invariant with respect to internal flow rates, reaction rates, temperatures and pressures. It is shown that $STCB$ is only dependent on the input fuel flow rate and current draw through simple algebraic relationships. Using invariant relationships, the steady-state fuel utilization and $STCB$ can be maintained at a target value and its transient fluctuations can be attenuated.

¹The contents of this chapter have been previously published [68]

2.2 Analysis of Steady-State Steam to Carbon Balance

2.2.1 Definition and Significance of STCR

Carbon deposition which is a common issue in SOFCs [37, 38], can be jeopardizing the health of catalysts in both reformer and anode [69]. Many works has been done by researchers to address this issue. While some have developed control strategies that are sensitive with respect to carbon deposition [70], Others have focused on different types of fuels other than H_2 [71, 72]. Another case in point is to control the carbon deposition using *STCR*. While U is a vital parameter determining the health of fuel cell, Steam-To-Carbon-Ratio (*STCR*) plays similar role in the reformer. The effect of *STCR* on the performance of SOFC has been experimentally investigated in [73]. On the other hand, *STCR* seems to be a rather complicated variable to control. With the aid of simulation, authors in [74] have shown that several fuel cell variables have significant effect of the *STCR*. Moreover, it was observed that there are considerable nonlinearities between the *STCR* and certain variables including inlet fuel pressure and system pressure [74]. Therefore, to ensure having sufficient steam to react with Carbon atoms preventing deposition, steam to carbon ratio (STCR) is defined as follows:

$$STCR \triangleq \frac{\text{Net amount of Steam at the Inlet of SR}}{\text{Net amount of Carbon Atoms at the Inlet of SR}} \quad (2.1)$$

Therefore, Referring to Fig.1.1 and Eq.(2.1), for a Methane based steam reformer, $STCR$ is defined as

$$STCR = \frac{k\dot{N}_o\mathcal{X}_{5,a} + \dot{N}_{st}\mathcal{X}_{st}}{\dot{N}_f + k\dot{N}_o\mathcal{X}_{1,a} + k\dot{N}_o\mathcal{X}_{2,a}} \quad (2.2)$$

As is indicated by Eq.(2.2)[1], $STCR$ is the ratio of the concentration of steam molecules to that of carbon atoms at the inlet of the reformer. It is noteworthy that $STCR$ is an important factor in determining the health of the reformer. Similarly, fuel utilization U can be used as an index of the health of the fuel cell stack. Therefore, while it is highly important to maintain U within limits, it is equally important to monitor $STCR$ to guarantee the performance of the reformer.

Based on Eq.(1.1), it is evident that the stoichiometric quantity of steam required for reforming 1 mole of CH_4 and CO is 2 moles and 1 mole, respectively. With this observation, for a Methane based SR, authors in [1] defined a new variable called steam to carbon balance (STCB) as follows:

$$\begin{aligned} STCB &= k\dot{N}_o\mathcal{X}_{5,a} + \dot{N}_{st}\mathcal{X}_{st} - (2\dot{N}_f + 2k\dot{N}_o\mathcal{X}_{1,a} + k\dot{N}_o\mathcal{X}_{2,a}) \\ &= k\dot{N}_o(\mathcal{X}_{5,a} - 2\mathcal{X}_{1,a} - \mathcal{X}_{2,a}) + \dot{N}_{st}\mathcal{X}_{st} - 2\dot{N}_f \end{aligned} \quad (2.3)$$

Essentially, $STCB$ represents the total amount of steam provided to the reformer, subtracted by the total amount of steam potentially consumed by both fuel and recirculated flow. Similar to $STCR$, all the calculations for the $STCB$ are taking place at the inlet of reformer. With that being said, one can conclude that a positive value of $STCB$ is desirable to prevent

carbon deposition [1].

Moreover, based on Eqs.(2.2),(2.3), it can be inferred that while the *STCR* is dependent on the reaction rates, the *STCB* is defined such that it is independent of reaction rates. For instance, a higher reaction rate for consumption of more hydrocarbons in anode will lead into production of more steam and that will keep the balance of steam and carbons the same. This independence from reaction rates, enables *STCB* as an “Invariant Property”, whereas *STCR* does not show the same quality. Therefore, *STCB* can replace *STCR* as a measure to monitor the health of the reformer. In the following discussion, we will prove that Steady-State *STCB* is an “Invariant Property”. we rewrite Eq.(2.3) using the following coordinate transformations:

$$\begin{aligned} STCB = k\dot{N}_o\xi_a - 2\dot{N}_f, \quad \xi_r &= \mathcal{X}_{5,r} - 2\mathcal{X}_{1,r} - \mathcal{X}_{2,r} \\ \xi_a &= \mathcal{X}_{5,a} - 2\mathcal{X}_{1,a} - \mathcal{X}_{2,a} \end{aligned} \quad (2.4)$$

Using Eqs.(1.5), (1.12) and (2.4), ξ_r and ξ_a can be expressed as

$$N_r\dot{\xi}_r = -\dot{N}_{in}\xi_r + k\dot{N}_o\xi_a - 2\dot{N}_f, \quad N_a\dot{\xi}_a = \dot{N}_{in}\xi_r - \dot{N}_o\xi_a + i\mathcal{N}_{cell}/nF \quad (2.5)$$

From Eq.(2.5), we obtain the following steady-state expression for *STCB* which is invariant with respect to temperatures, pressures, and reaction rates.

$$STCB_{ss} = \frac{1}{k-1} \left(2\dot{N}_f - \frac{ki\mathcal{N}_{cell}}{nF} \right) \quad (2.6)$$

2.2.2 General Steady-State Expression of STCB for SR-SOFC System

In this section, we perform some matrix analysis on STCB which was similarly applied on U in [75, 68]. We first, introduce the conservation of mass for an individual species in a generic gas control volume, denoted by subscript g , can be derived from first principles as:

$$\frac{d}{dt}(N_g X_{j,g}) = \dot{N}_{en} X_{j,en} - \dot{N}_{ex} X_{j,g} + \mathcal{R}_{j,g} \quad (2.7)$$

where, $j = 1, 2, 3, \dots$ represents individual species in the gas flow. $\mathcal{R}_{j,g}$ is the net rate of formation of species j in mol/s due to all chemical reactions in the control volume. The subscripts en and ex denote the streams entering and exiting the control volume respectively. It is assumed that the stream leaving the control volume and the control volume itself have the same composition $X_{j,g}$, $j = 1, 2, 3, \dots$. The conservation of mass equation for the gas mixture is obtained from Eq.(2.7),

$$\frac{d}{dt}(N_g \mathbf{X}_g) = \dot{N}_{en} \mathbf{X}_{en} - \dot{N}_{ex} \mathbf{X}_g + \mathbf{R}_g \quad (2.8)$$

where,

$$\mathbf{X}_g = [X_{1,g} \ X_{2,g} \ X_{3,g} \ \dots]^\top, \quad \mathbf{X}_{en} = [X_{1,en} \ X_{2,en} \ X_{3,en} \ \dots]^\top, \quad \mathbf{R}_g = [\mathcal{R}_{1,g} \ \mathcal{R}_{2,g} \ \mathcal{R}_{3,g} \ \dots]^\top \quad (2.9)$$

In Eq.(2.9), it is noted that the indices $1, 2, 3, \dots$, represent individual species in the gas flow and hence the same sequence is used to present species molar fractions in vectors \mathbf{X}_g and

\mathbf{X}_{en} . On The other hand, to represent $STCB$ in a matrix form, we define a Q matrix such that

$$STCB = k\dot{N}_o\mathbf{Q}^T\mathbf{X}_o + \dot{N}_{st}\mathbf{Q}^T\mathbf{X}_{st} + \dot{N}_f\mathbf{Q}^T\mathbf{X}_f \quad (2.10)$$

where for the case of Methane-based SR, \mathbf{Q} can be found as

$$\mathbf{Q}^T = [-2 \quad -1 \quad 0 \quad 0 \quad 1] \quad (2.11)$$

By definition, \mathbf{Q} is a column vector containing the net available steam subtracted by the potential steam consumed by Carbon atoms. Next, we attempt to obtain the steady-state $STCB$ by focusing on the mass balance of the reformer and Anode control volumes. The mass balance of the available steam in the gas control volume can be found by pre-multiplying Eq.(2.8) with \mathbf{Q}^T . This results in an equation for the conservation of mass of *Available Steam* as follows,

$$\dot{N}_g\mathbf{Q}^T\mathbf{X}_g + N_g\mathbf{Q}^T\dot{\mathbf{X}}_g = \dot{N}_{en}\mathbf{Q}^T\mathbf{X}_{en} - \dot{N}_{ex}\mathbf{Q}^T\mathbf{X}_g + \mathbf{Q}^T\mathbf{R}_g \quad (2.12)$$

Considering steady-state conditions, the left hand side of Eq.(2.12) goes to zero, giving

$$0 = \dot{N}_{en}\mathbf{Q}^T\mathbf{X}_{en} - \dot{N}_{ex}\mathbf{Q}^T\mathbf{X}_g + \mathbf{Q}^T\mathbf{R}_g \quad (2.13)$$

Next Eq.(2.13) will be applied for SR and anode control volumes and then in conjunction with Eq.(2.10) will yield an expression for the steady-state $STCB$.

As was mentioned before, considering the SR control volume, there are three inlet flows, the

pre-reformed fuel \dot{N}_f with species concentrations \mathbf{X}_f which is considered known, steam \dot{N}_{st} with concentrations \mathbf{X}_{st} where the entries of this vector are zero excepting for the entry corresponding to concentration of steam which is 1, and $k\dot{N}_o$ with concentrations \mathbf{X}_o . Applying Eq.(2.13) for SR control volume gives:

$$0 = \dot{N}_f \mathbf{Q}^T \mathbf{X}_f + \dot{N}_{st} \mathbf{Q}^T \mathbf{X}_{st} + k\dot{N}_o \mathbf{Q}^T \mathbf{X}_o - \dot{N}_{in} \mathbf{Q}^T \mathbf{X}_{in} + \mathbf{Q}^T \mathbf{R}_{SR} \quad (2.14)$$

where \mathbf{R}_{SR} represents a column vector containing rate of formation of each species through steam reforming reactions. We next make the following observation. *The chemical reactions in the SR do not change the total steam available in the gas mixture, they only change the form from higher hydrocarbons to lower hydrocarbons and hydrogen molecules.* Hence, assuming \mathbf{Q} is formulated correctly, $\mathbf{Q}^T \mathbf{R}_{SR} = 0$. This simplifies Eq.(2.14) to,

$$0 = \dot{N}_f \mathbf{Q}^T \mathbf{X}_f + k\dot{N}_o \mathbf{Q}^T \mathbf{X}_o + \dot{N}_{st} \mathbf{Q}^T \mathbf{X}_{st} - \dot{N}_{in} \mathbf{Q}^T \mathbf{X}_{in} \quad (2.15)$$

When applying Eq.(2.13) to the anode, $\mathbf{R}_g = \mathbf{R}_a$ will be a column vector containing the rates of formation of all species. The reactions include both the electrochemical reaction Eq.(1.7) and internal steam-reforming reactions. Hence

$$\mathbf{R}_g = \mathbf{R}_a = \mathbf{R}_{a,SR} + \mathbf{R}_{a,e} \Rightarrow \mathbf{Q}^T \mathbf{R}_g = \mathbf{Q}^T \mathbf{R}_a = \mathbf{Q}^T \mathbf{R}_{a,SR} + \mathbf{Q}^T \mathbf{R}_{a,e} = \mathbf{Q}^T \mathbf{R}_{a,e} = r_e \quad (2.16)$$

where $\mathbf{R}_{a,SR}$ and $\mathbf{R}_{a,e}$ contain the rates of internal steam reforming reactions and electrochemical reactions respectively. Eq.(2.16) is valid because the only chemical reaction that affects total steam in the flow is the electrochemical reaction. Equation (2.13) thus reduces to

$$0 = \dot{N}_{in} \mathbf{Q}^T \mathbf{X}_{in} - \dot{N}_o \mathbf{Q}^T \mathbf{X}_o + r_e \quad (2.17)$$

From Eqs.(1.9), (2.15), (2.17) and Eq.(2.10), the steady-state $STCB$ is expressed as

$$STCB_{ss} = \frac{1}{1-k} [\dot{N}_f \mathbf{Q}^T \mathbf{X}_f + \dot{N}_{st} \mathbf{Q}^T \mathbf{X}_{st} + \frac{ki\mathcal{N}_{cell}}{\mathbf{n}F}] \quad (2.18)$$

Note that in Eq.(2.18), i , \dot{N}_f , \dot{N}_{st} are inputs and \mathcal{N}_{cell} , \mathbf{n} , F , k and \mathbf{X}_f are known quantities. Hence, if the vector \mathbf{Q} can be obtained, then one can predict $STCB_{ss}$ for any set of input conditions for an SR-SOFC system without knowledge of the rates of reforming reactions, internal flow rates, temperatures and pressures.

2.3 Control of Fuel Cell Using Invariant Property

2.3.1 Control Scheme Via $STCB_{ss}$

Transient Control of SOFC system based on the constant U has been previously discussed in section 1.2.4. Similar to that discussion, $STCB_{ss}$ expression can replace the U_{ss} to regulate the current based on the fuel rate \dot{N}_f and $STCB_{ss}$. In other words:

$$\dot{N}_f = g_{IR}(STCB_{ss})i_{fc} \quad (2.19)$$

where for the Methane-based SR-SOFC system, Eq.(2.19) translates into:

$$\dot{N}_f = \frac{1}{2}[(k - 1)STCB_{ss} + ki \frac{\mathcal{N}_{cell}}{nF}] \quad (2.20)$$

Inverting Eq.(2.20) will yield the expression for the shaped FC current draw which guarantees operation at a pre-specified $STCB_{ss}$ value. Simulation results demonstrated in Fig.2.1 shows how the SOFC system behaves under the $STCB$ -based current regulation approach.

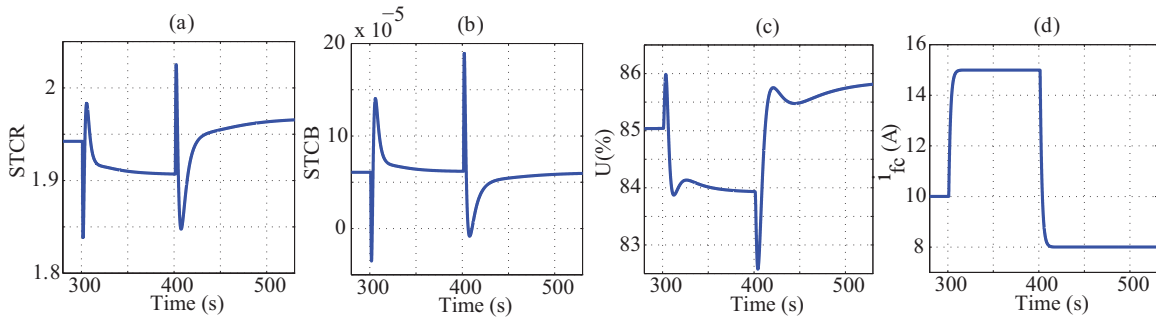


Figure 2.1: Simulation Results for $STCB$ -Based Current Regulation Approach

Comparing Fig.2.1 and Fig.2.2 (a)-(c) which depicts simulation results using U_{ss} -based current regulation, it can be deduced that system looks more stable using U_{ss} -based current regulation. In other words, while $STCB$ and $STCR$ look completely under control in both approaches, U seems to be not very stable in the $STCB$ -based approach. This observation can be attributed the the nonlinear nature of the U which mandates a proper control scheme to make it under control. Thus, the U_{ss} approach which was briefly discussed in section 1.2.4, and extensively discussed in [3] is a better control scheme compared to the $STCB$ -based method.

2.4 Performance Criteria for the Reformer and Fuel Cell Stack

2.4.1 STCR and STCB at the Stack

Before going into further details, one could raise the same concern of the possibility of carbon deposition inside the stack (anode). That is to say, how can we guarantee that there is enough steam to prevent carbon deposition inside the anode as the same species exist in the anode as well. To respond, we define the *STCR* at the anode as follows:

$$STCR_a \triangleq \frac{\text{Net amount of Steam at the Inlet of Anode}}{\text{Net amount of Carbon Atoms at the Inlet of Anode}} \quad (2.21)$$

Please note that while the major content of *CH4* and *CO* has been consumed in the SR, in addition to the steam that is fed to the stack by the SR exhaust flow, the electrochemical reaction is constantly producing steam which is favorable from the *STCR* and *STCB* standpoint. Therefore, for a Methane based steam reformer, *STCR* at the anode is defined as

$$STCR_a = \frac{\dot{N}_i n \mathcal{X}_{5,r} + r_e \mathcal{X}_{st}}{\dot{N}_i n \mathcal{X}_{1,r} + \dot{N}_i n \mathcal{X}_{2,r}} \quad (2.22)$$

Similarly, *STCB* at the anode can be defined as:

$$STCB_a = \dot{N}_i n \mathcal{X}_{5,r} + r_e \mathcal{X}_{st} - 2\dot{N}_i n \mathcal{X}_{1,r} - \dot{N}_i n \mathcal{X}_{2,r} \quad (2.23)$$

It can be predicted based on Eqs.(2.22), and (2.23) that there is a considerable margin of safety in the anode with respect to *STCR* and *STCB*. Convincingly, the Simulation

results depicted in Fig.2.2 demonstrate that for a Methane-based SR with no external steam injection, the necessity of monitoring $STCB$ in the SR is much more compared to that of the stack as for even a small step change in current draw, $STCB_{SR}$ falls below zero which is detrimental to the health of the SR.

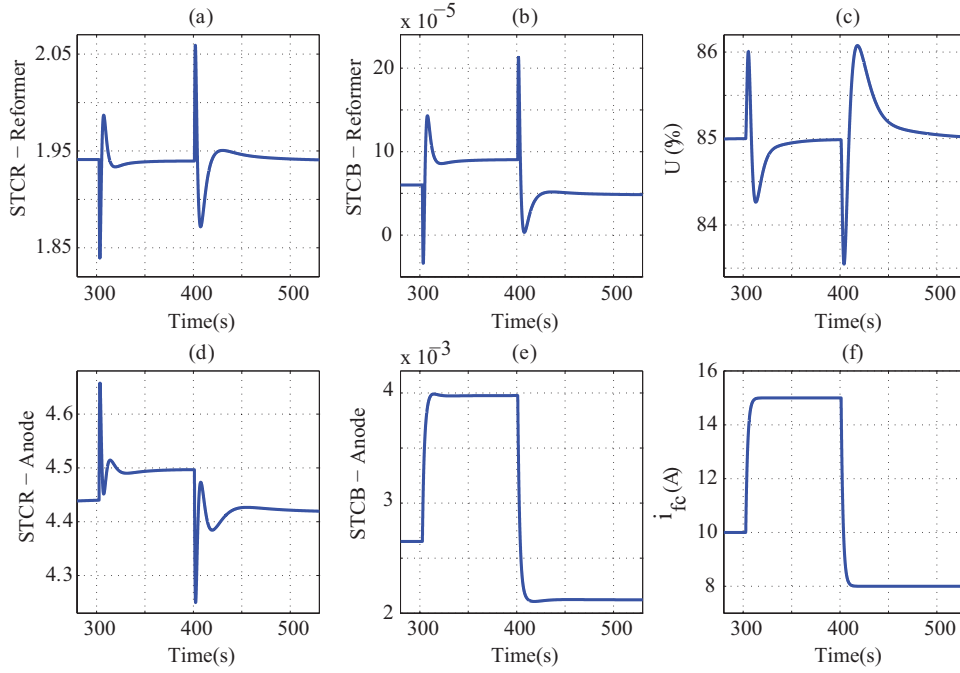


Figure 2.2: Comparison of STCR and STCB for Both Reformer and Stack

2.4.2 Performance Challenges

As is mentioned in section 1.2.4, U_{ss} expression is employed to shape the current based on the actual fuel flow, given a fixed U_{ss} value. This way, while operating at constant steady state fuel utilization, the fluctuations of the U is minimized and the health of the fuel cell stack is guaranteed during even significant transients. However, to make sure the reformer is also operating in the safe region, it is vital to ensure $STCB$ lies within the acceptable range.

First, given the control strategy detailed at section 1.2.4, to ensure constant U_{ss} , the following needs to be satisfied:

$$U_{ss} = \frac{1 - k}{(\mathbf{n}F\dot{N}_f\mathbf{P}^\top\mathbf{X}_f/i\mathcal{N}_{cell}) - k} \quad (2.24)$$

In other words, since \mathbf{n}, F, k , and \mathcal{N}_{cell} are all constants, to maintain a fixed U_{ss} ,

$$\dot{N}_f\mathbf{P}^\top\mathbf{X}_f/iD = C_1 = \text{const.} \quad (2.25)$$

where $D = \mathcal{N}_{cell}/\mathbf{n}F$ is a constant. On the other hand, referring to Eq.(2.18), assuming no external steam feeding, to keep a fixed $STCB_{ss}$,

$$\dot{N}_f\mathbf{Q}^\top\mathbf{X}_f + \dot{N}_{st}\mathbf{Q}^\top\mathbf{X}_{st} + kiD = C_2 = \text{const.} \quad (2.26)$$

Therefore, simplifying Eq.(2.26) using Eq.(2.25),

$$\dot{N}_f\mathbf{Q}^\top\mathbf{X}_f + \frac{k}{C_1}\dot{N}_f\mathbf{P}^\top\mathbf{X}_f + \dot{N}_{st}\mathbf{Q}^\top\mathbf{X}_{st} = C_2 = \text{const.} \quad (2.27)$$

Since all the components in the Eq.(2.27) are constant except \dot{N}_f , and \dot{N}_{st} , it is evident that Eq.(2.27) cannot hold true. Therefore, with the current control methodology that keeps U_{ss} at a fixed value, $STCB_{ss}$ cannot be fixed. Therefore, the challenge is to find a way that can guarantee the healthy performance of both reformer and Stack at the same time.

2.4.3 Healthy Performance Criteria

Referring to Fig.2.2(b), and(e), it can be seen that the $STCB_{SR}$ and U behave in the opposite manners. That is, increasing one leads into decreasing the other and vice versa; thus, controlling both at the same time can serve as conflicting objectives. Another observation is that the critical condition where $STCB_{SR}$ falls and U rises happens as a consequence of increasing the current draw from the FC. Both of these observations can be justified by looking at our control methodology. That is, since the current regulation method described in Sec. 1.2.4 is based on delaying the current drawn from the fuel cell based on the actual fuel flow, this will first cause the fuel flow to increase and with some further lag, the current produced by FC will also increase. Therefore, any change in the current demand will first affect the fuel flow, and subsequently, that will be reflected in the actual current produced in the FC. For instance, referring to Fig.2.2(b), (d) and(e), a current step change from 10 to 15A will first cause increasing fuel flow in the reformer. That will make $STCB$ to fall, and U to rise because the added fuel has not broken into hydrogen yet; however, the increase in current draw means more electricity must be generated and consequently, more steam will be generated that will be recirculated back to the reformer and make the $STCB$ to back up. Furthermore, more steam and more fuel in the reformer means more hydrogen is fed into the anode and that will make U to fall back to its steady state value again.

In order to improve the response of the system during the transients, one could argue that further lagging the current draw from the fuel cell can decrease transient overshoot and

undershoot and be eventually favorable. Fig. 2.3 demonstrates the simulation results for the previous system using a first order filter with a time constant of $\tau = 2s$ acting upon current.

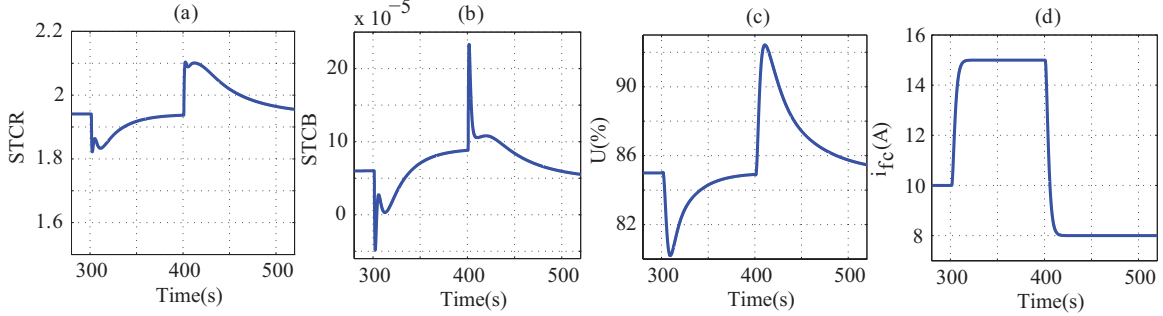


Figure 2.3: Simulation Results for U -Based Current Regulation Approach with Lagged Current

However, the filter on the current turned out to have an adverse effect on the system as it not only increased the type of the system to the second order, it increased amount of undershoot and overshoot of both $STCB$ and U due to slow response of the system.

To address the challenge expressed in the preceding section, our objective is to make sure $STCB_{ss} \geq 0$ at all time. Granted, this does not guarantee the $STCB$ not crossing 0 at all, yet, that issue can be easily solved using an external steam injection into the reformer during the transients. Therefore, for a Methane-based steam reformer with no external steam feed we have:

$$STCB_{ss} \geq 0 \Rightarrow \dot{N}_f \leq k\left(\frac{i\mathcal{N}_{cell}}{2nF}\right) \quad (2.28)$$

On the other hand, we have

$$U_{ss} \geq 0 \Rightarrow \dot{N}_f \geq k\left(\frac{i\mathcal{N}_{cell}}{4nF}\right) \quad (2.29)$$

Combining Eqs.(2.28), (2.29), and $0 < U_{ss} < 1$ will construct a set of linear inequalities which is solved in a prior publication [1] from another perspective. In [1], the focus of others was fuel optimization whereas here, the focus is ensuring a healthy performance for both SR and stack. Referring to [1], it is concluded that to ensure $STCB_{ss} \geq 0$ and $U_{ss} = Const.$, it is necessary to have the following condition satisfied:

$$k \geq \frac{1}{1 + U_{ss}} \quad (2.30)$$

That is to say, the recirculation ratio k needs to be tuned based on the U_{ss} to have a safe performance. This condition will guarantee a positive steady state $STCB$ without the aid of any external steam feeding.

2.5 Chapter Summary

In this chapter, it was shown that in order to avoid carbon deposition in the reformer of SOFC systems, it is vital to maintain $STCR$ at a certain level. Therefore, using the concept of conservation of potential steam, $STCB$ was introduced and proved to be invariant with respect to majority of operating conditions. Moreover, a general analysis was performed to obtain the steady state expression of $STCB$ which is valid for all types of reformer based SOFCs. It was shown through simulations that the problem of carbon deposition does not exist in anode due to electrochemical reaction. Furthermore, a control scheme using the $STCB_{ss}$ expression was outlined and compared to the aforementioned utilization based

control strategy. Finally, the conditions guaranteeing simultaneous safe operation of SOFC stack and reformer were discussed.

CHAPTER 3

TRANSIENT CONTROL IN MULTIVARIABLE SYSTEMS WITH APPLICATION IN SOFC

1

3.1 Chapter Overview

Controlling the transient response of variables for which sensing or accurate estimation is not feasible, and a detailed plant model is also largely unavailable, poses significant challenges. It is a situation that is true in solid oxide fuel cells. In SOFCs, transient control is essential for fuel utilization, especially if the fuel cell is to be operated in a dynamic load-following mode at high fuel utilization. The objective is to design the control input(s) such that it isolates the output (fuel utilization in this case) from measurable disturbances, while the plant itself maybe largely unknown. The features assumed known are the output's functional dependence on states which is essentially the output definition, and the steady-state equation relating the multiple inputs and the output of interest. Simulations have shown good disturbance rejection in fuel utilization through input shaping. This idea is abstracted to linear multi-variable systems to provide conditions when this approach is applicable. The analysis is carried out in time-domain as well as in frequency domain (through singular value

¹The contents of this chapter have been previously published [76].

analysis). The type of output variables that are amenable to transient control using this approach is derived through analysis. It is shown that the fuel utilization, although inherently nonlinear within the nonlinear dynamics of the fuel cell, has some similarities with the linear abstraction that leads to the observed transient control.

3.2 Output Controllability

3.2.1 What is Output Controllability?

In the control theory, controllability is a common concept which is usually defined as the ability of a system to reach any desired state starting from any initial state within a finite period of time [77]. However, in many engineering applications, it is needed to direct the output toward some desired value. In fact, having control over the output of the system has a significant importance if not more than the states. Reviewing the literature, it is shown that no obvious connection can be verified between state controllability and output controllability [78, 79].

For a LTI (Linear Time Invariant) system with constant coefficients, controllability can be defined as follows:

Definition 2.1: *A dynamic system*

$$\dot{X}(t) = AX(t) + Bu(t), \quad y(t) = CX(t) \quad (3.1)$$

where, $A \in \mathbb{R}^{n \times n}$, $B \in \mathbb{R}^{n \times m}$, $C \in \mathbb{R}^{p \times n}$; is called controllable if for any initial state $X(0)$ and any vector $X_1 \in \mathbb{R}^n$, there exists a finite time t_1 and control $u(t) \in \mathbb{R}^m, t \in [0, t_1]$ such

that $X(t_1) = X_1$ [80].

In order to verify the controllability of a system, it is conventional to construct the following matrix

$$C_o = \begin{bmatrix} B & AB & A^2B & \dots & A^{n-1}B \end{bmatrix} \quad (3.2)$$

It can be mathematically proved that the dynamic system 3.1 is controllable if and only if rank of $C_o = n$ [80, 77].

On the other hand, the concept of “Output Controllability” was first introduced by Brockett in [81] as “Reproducibility” of the system. By definition, reproducibility refers to the capability of a system to reach some desired output [81]. In this regard, many different forms of reproducibility has been defined and discussed on such as functional reproducibility which refers to the ability of a system to generate some particular time functions; asymptotic reproducibility which is related to the likelihood of reaching a specified behavior over time; and point-wise reproducibility which implies the possibility of approaching some pre-specified value of the output subspace at some point in time [81].

In general, the output controllability means that the system’s output can be directed regardless of its state [82]. According to Brockett, the least restrictive form of reproducibility is called pointwise reproducibility which is defined as follows:

Definition 2.2: *The homogenous response from an initial state α is called pointwise reproducible if for any $\beta > 0$ and a finite time $\tau > 0$ there exists a $\delta(\beta, \tau)$ such that corresponding*

to each output y for which

$$\|y - CX(\alpha, 0, t)\|_n < \delta(\beta, \tau) \quad (3.3)$$

there exists a control $\|u\| < \beta$ that mandates $CX(\alpha, u, t) = y(t)$ for at least one value of $t \in [0, \tau]$.

In fact, this is not very restrictive condition as many dynamic systems possess this property and yet, are not “controllable” in practice [81]. Analogous to state controllability, output controllability for the LTI systems can be also defined as follows:

Definition 2.3: *The dynamic system 3.1 is called output controllable or pointwise reproducible if for any initial output $y(0)$ and any vector $y_1 \in \mathbb{R}^p$, there exists a finite time t_1 and control $u_1(t) \in \mathbb{R}^m, t \in [0, t_1]$ such that transfers the output from $y(0)$ to $y_1 = y(t_1)$ [80].*

Similarly, a simple test for verifying output controllability can be obtained by constructing the following matrix

$$o_C = \begin{bmatrix} CB & CAB & CA^2B & \dots & CA^{n-1}B \end{bmatrix} \quad (3.4)$$

It is mathematically proved that the dynamic system 3.1 is output controllable if and only if rank of $o_C = p$ [80].

It is noteworthy that the state controllability is dependent on linear differential equation of states; whereas the output controllability is not only dependent on differential equation of states, it also is related to the algebraic output equation [80].

3.2.2 Functional Output Controllability

Generally speaking, the functional output controllability is related to the ability of a system to direct its output toward any arbitrary curve over any period of time, regardless of its states. That is, if it is given a desired output $y_d(t), t \geq 0$, there exists some t_1 and a control $u_t, t \geq 0$ such that it mandates $y(t) = y_d(t)$ for any $t \geq t_1$ [82].

Mathematically speaking, functional output controllability, i.e. reproducibility can be defined as follows:

Definition 2.4: *The homogenous response from an initial state α is called functionally reproducible if for any $\beta > 0$ and a finite time $\tau > 0$ there exists a $\delta(\beta, \tau)$ such that corresponding to each output y for which*

$$\|y - CX(\alpha, 0, t)\|_n < \delta(\beta, \tau) \tag{3.5}$$

there exists a control $\|u\| < \beta$ that mandates $CX(\alpha, u, t) = y(t)$ for all values of $t \in [0, \tau]$ [81].

In general, functional reproducibility is a local property as in the above definition, the behavior of the dynamic system in the vicinity of the desired solution is investigated.

3.2.2.1 Functional Output Controllability in LTI systems

The following theorem which is introduced and proved in [81] expresses the condition for functional reproducibility or functional output controllability.

Theorem 2.1: *Consider the LTI system 3.1 for which all the assumptions for A , B , and C hold true; All homogeneous responses of this system are functionally reproducible if and only if the $pn \times (2mn - m)$ matrix*

$$M_n = \begin{bmatrix} CB & CAB & CA^2B & \dots & CA^{n-1}B & CA^nB & \dots & CA^{2n-1}B \\ 0 & CB & CAB & \dots & CA^{n-2}B & CA^{n-1}B & \dots & CA^{2n-2}B \\ 0 & 0 & CB & \dots & CA^{n-3}B & CA^{n-2}B & \dots & CA^{2n-3}B \\ \vdots & \vdots & \vdots & \dots & \vdots & \vdots & \dots & \vdots \\ 0 & 0 & 0 & \dots & CB & CAB & \dots & CA^{n-1}B \end{bmatrix} \quad (3.6)$$

is of rank pn [81].

Similarly, in [82], the following condition is introduced as the necessary and sufficient condition for functional output controllability.

$$\text{rank} \begin{bmatrix} C \\ CA & CB \\ CA^2 & CAB & CB \\ \vdots & \dots & \ddots \\ CA^n & CA^{n-1}B & \dots & CAB & CB \end{bmatrix} = (n+1)p \quad (3.7)$$

In the frequency domain, it is shown by Brockett in [81] that $C(Is - A)^{-1}B$ is of rank p if and only if M_n is of rank pn . Analogously, if

$$\text{rank} \begin{bmatrix} sI - A & B \\ C & 0 \end{bmatrix} = n + p \quad (3.8)$$

the system (A, B, C) is functionally output controllable [82].

Proposition: *Consider the following singular system*

$$E\dot{X}(t) = AX(t) + Bu(t), \quad y(t) = CX(t) \quad (3.9)$$

where $E \in \mathbb{R}^{n \times n}$. This singular system is functional output controllable if and only if

$$\text{rank} \begin{bmatrix} sE - A & B \\ C & 0 \end{bmatrix} = n + p \quad (3.10)$$

or rank of $C(sE - A)^{-1}B = p$ [82].

3.2.3 Steady-State Output Controllability

By definition, for system 3.1, if a control vector U is provided such that

$$\lim_{t \rightarrow \infty} y(t) = \delta \quad (3.11)$$

where δ is a $p \times 1$ output vector, and δ_i is a given constant, then this problem is called constant steady-state output controllability of LTI systems [78, 80].

Definition 2.5: *An LTI system like 3.1 is claimed to be steady state output controllable if an input vector $U(s)$ where $u_i(s) = \frac{k_i}{s}$ can be found that generates a constant desired output vector δ [78, 80].*

Clearly, a mandatory pre-condition for constant steady-state output controllability of the system is stability of the system [80].

Proposition: *A stable system like 3.1 is constant steady-state output controllable if and only if [80]*

$$\text{rank} \begin{bmatrix} A & B \\ C & 0 \end{bmatrix} = n + \min[m, p] \quad (3.12)$$

3.2.4 Output Controllability in Nonlinear Systems

Brockett in [81] has established a method for checking the reproducibility of nonlinear systems by testing its linear terms under some specific conditions.

Consider A, B and C matrices similar to system 3.1; and consider A is Hurwitz. Let $M(a)$ denote the point set $\{X(t), U(t) : |X(t)| < a, |U(t)| < a\}$. Consider the following nonlinear system

$$\begin{aligned} \dot{X}(t) &= AX(t) + BU(t) + BR(X(t), U(t)) \\ y(t) &= CX(t) \end{aligned} \quad (3.13)$$

where $R(X(t), U(t))$ and its partial derivatives with respect to the components of $X(t)$ and $U(t)$ are continuous in $N(a)$ and disappear when $X(t)$ and $U(t)$ disappear. Then, the

following theorem can be proved.

Theorem 2.2: *Consider the system 3.13 with the given assumptions on all its components.*

Therefore, there exists a $\beta > 0$ such that any homogeneous response of the form $CX(\eta, 0, t)$ with $|\eta| < \beta$ is i) pointwise, or ii) functionally reproducible if all the homogeneous responses of the linearized system

$$\begin{aligned} \dot{X}(t) &= AX(t) + BU(t) \\ y(t) &= CX(t) \end{aligned} \tag{3.14}$$

are i) pointwise, or ii) functionally reproducible [81].

3.3 A Generalized Transient Control Problem

From the pre-outlined transient control problem of Solid Oxide Fuel Cells in section 1.3, a generalized transient control problem can be formulated for multi-input single output (MISO) systems. This generalized problem statement is as follows: Consider a nonlinear and non-autonomous MISO system described as,

$$\dot{X} = f(X, t, u, w), \quad y = h(X, t, u, w) \tag{3.15}$$

where, X is the state vector, y is the output, u is the vector of control inputs and w is the vector of disturbance/exogenous inputs. Let us assume that at steady-state,

$$y_{ss} = g(u_{ss}, w_{ss}) \tag{3.16}$$

where the subscript ss denotes steady-state. Further, let us assume that the following are true:

1. The functions $h(X, t, u, w)$ and $g(u_{ss}, w_{ss})$ are known but knowledge of $f(X, t, u, w)$ is “incomplete”.

Note: The exact implication of “incomplete” knowledge of the plant will be clarified in the problem statements in the following sections.

2. X and y are not measurable, but the exogenous inputs w are measurable.

Then, under what additional condition(s), can we design the control inputs $u = q(w)$ such that $\lim_{t \rightarrow \infty} y(t) = \delta$, where δ is a desired/target value of y ?

The above problem corresponds closely to the fuel utilization control problem in SOFCs, where X corresponds to the states and y corresponds to U , whose functional form is known as well. Also, \dot{N}_{in} , \dot{N}_o , N_r , N_a , are functions of time, making the system non-autonomous. \dot{N}_f is the exogeneous input and i_{fc} , which is shaped based on \dot{N}_f using Eq.(1.19), is the control input. Eq.(1.17) corresponds to the function $g(u_{ss}, w_{ss})$, assumed known. Also, δ corresponds to the target U_{ss} . We first formulate the problem for a linear time invariant(LTI) MISO system.

3.4 Problem Formulation for an LTI-MISO System

Consider the following LTI-MISO system

$$\dot{X} = AX + B(u + w), \quad y = CX \tag{3.17}$$

where $A \in \mathbb{R}^{n \times n}$, $B \in \mathbb{R}^{n \times n}$, $C \in \mathbb{R}^{1 \times n}$. Also let $u \in \mathbb{R}^{n \times 1}$ and $w \in \mathbb{R}^{n \times 1}$ represent the vectors containing the control inputs and disturbance inputs respectively. Following to Eq.(3.17), the steady-state input/output relation is therefore

$$\begin{aligned}
 \dot{X}_{ss} &= 0 = AX_{ss} + B(u_{ss} + w_{ss}) \\
 \Rightarrow X_{ss} &= -A^{-1}B(u_{ss} + w_{ss}) \\
 \Rightarrow y_{ss} &= CX_{ss} = -CA^{-1}B(u_{ss} + w_{ss})
 \end{aligned} \tag{3.18}$$

Next, we make the following assumptions that are parallel to those for the generalized non-linear time-varying case:

1. B and C matrices are known but A is unknown.
2. A is Hurwitz which can be inferred based on an overall physical knowledge of the system.
3. B is invertible.
4. There are $m < n$ disturbance inputs in w and $(n - m) \geq 1$ control inputs in u . This implies that the sum of L_0 “norms” of u and w is n , which essentially means a total of n inputs.
5. $CA^{-1}B$ is known.

Note: Knowing C , B and Eq.(3.18) does not imply the knowledge of A .

6. X and y are not measurable, but the exogenous inputs w are measurable.

Note that the set of assumptions above now clearly defines what we mean by incomplete knowledge of $f(X, t, u, w)$ in assumption 1 of the generalized case, but this definition is only applicable for LTI-MISO systems. The question we ask is, can we design $u = q(w)$ such that $\lim_{t \rightarrow \infty} y(t) = \delta$ where δ is a desired/target value? To this end, we give the following theorem:

THEOREM 1: *Consider the LTI system given in Eq.(3.17) for which all the above assumptions are valid. If y is such that CA^{-1} and C are linearly dependent, then by using Eq.(3.18) with*

$$\delta = -CA^{-1}B(u + w) \quad (3.19)$$

we can completely eliminate the effect of w on y and ensure $\lim_{t \rightarrow \infty} y(t) = \delta$ for any transients in w .

Proof: First, we observe that since C , B and $CA^{-1}B$ are known and B is invertible, CA^{-1} can be determined from the given information. Hence we can verify if C and CA^{-1} are linearly dependent, without knowing A . If they are, then

$$CA^{-1} = \alpha C, \quad \alpha < 0 \quad (3.20)$$

Here $\alpha < 0$ because Eq.(3.20) implies

$$C = \alpha CA \Rightarrow C \left(\frac{1}{\alpha} I - A \right) = 0 \quad (3.21)$$

and hence $1/\alpha$ is an eigenvalue of A and C is the corresponding eigenvector. Since A is known to be Hurwitz, α is negative real. Now, taking the derivative of Y , we have

$$\dot{y} = CAX + CB(u + w) \Rightarrow \dot{y} = \frac{1}{\alpha}y + CB(u + w) \quad (3.22)$$

which implies that by choosing u to satisfy

$$CB(u + w) = CBu + CBw = -\frac{\delta}{\alpha} \Rightarrow \lim_{t \rightarrow \infty} y(t) = \delta \quad (3.23)$$

From Eq.(3.20), $CA^{-1} = \alpha C$ and therefore by choosing u to satisfy

$$CA^{-1}B(u + w) = -\delta \quad (3.24)$$

we ensure $\lim_{t \rightarrow \infty} y(t) = \delta$. This completes the proof. $\diamond \diamond \diamond$

We note that we are essentially using the steady-state equation Eq.(3.18) to *shape* u using the measurements of w to ensure complete disturbance rejection in y . Also, given that w is measurable, we only need one control input to control the transients in y . Any extra control input can be used to achieve other control objectives. We also make the following observations:

Remark 1: *Given a MISO-LTI system with B , C and $CA^{-1}B$ satisfying all the conditions of Theorem 1, there exists a continuum of realizations of admissible A matrices.*

Remark 2: *A loss of observability is an enabler for transient control of y , since linear*

dependence of C and CA^{-1} implies a rank 1 observability matrix.

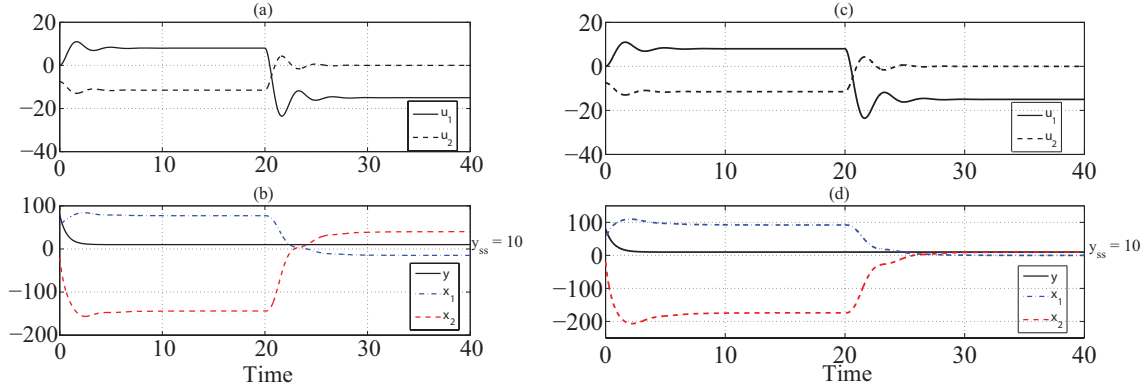


Figure 3.1: Simulation Showing Isolation Of y From Exogenous Input u_1 During Transients.

To illustrate the effectiveness of the Theorem 1, simulation results are shown in Fig.3.1(a),(b).

The system chosen in 3.1(a) is

$$A = \begin{bmatrix} 1 & 0.75 \\ -5 & -3 \end{bmatrix} \quad B = \begin{bmatrix} 1 & -2 \\ -3 & 2 \end{bmatrix} \quad C = \begin{bmatrix} 2 & 1 \end{bmatrix} \quad (3.25)$$

in which u_1 is considered an exogenous input and u_2 is the control input. Thus, $u = [u_1 \ 0]^T$ and $w = [0 \ u_2]^T$. The matrices B , C and $CA^{-1}B = [2/3 \ 4/3]$ are assumed known. A is Hurwitz (eigenvalues at -0.5 and -1.5) but is assumed unknown. It can be verified that B is invertible. Using B and $CA^{-1}B$, we can verify that $CA^{-1} = -(2/3)C$, implying $\alpha = -2/3$. Indeed, $1/\alpha = -1.5$ is an eigenvalue of A . We set the target $\delta = 10$. This implies from Eq.(3.19) that if u_2 satisfies

$$-CA^{-1}B [u_1 \ u_2]^T = -[2/3 \ 4/3] [u_1 \ u_2]^T = 10, \quad (3.26)$$

for any measured exogenous input u_1 , then $\lim_{t \rightarrow \infty} y(t) = 10$. This is confirmed in Fig.3.1(b). In this simulation, initial values $X(0) = [50 \quad -20]^T$ were chosen arbitrarily. At $t = 20$ s the disturbance input u_1 was changed from 8 to -15 with an underdamped second order dynamics. Note that u_2 is shaped using Eq.(3.26).

Moreover, to demonstrate what was mentioned in *Remark 1*, another simulation was run using a different A matrix with the same B and C and the same inputs (u_1 and u_2). In this case, system was chosen to be

$$A = \begin{bmatrix} 2.5 & 1.5 \\ -8 & -4.5 \end{bmatrix} \quad B = \begin{bmatrix} 1 & -2 \\ -3 & 2 \end{bmatrix} \quad C = \begin{bmatrix} 2 & 1 \end{bmatrix} \quad (3.27)$$

for which the same exact inputs are implemented. In Fig.3.2 we compare the transient performance of the system described in Eq.(3.25) with two different choices of C that are not linearly dependent on CA^{-1} . It can be seen from the Fig.3.2 that with only linearly dependent C , perfect transient response is achievable while for other options, some deviations from the steady state value can be observed.

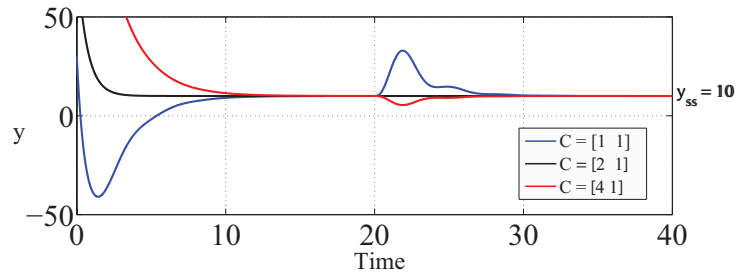


Figure 3.2: Comparison Of Transient Response For Three Different C Matrices.

3.4.1 Complex Conjugate case

So far, we showed the feasibility of transient control for the case where C and CA^{-1} are linearly dependent. This implies that the dependence is through a negative real eigenvalue; in other words, A must be Hurwitz. However, one could pose the same question for a case where A has complex conjugate yet stable eigenvalues. Now, the question arising from what we have discussed so far is: Considering an LTI-MISO system for which complex conjugate eigenvalues are present; Assuming all the aforementioned assumptions hold through, can we design $u = q(w)$ such that $\lim_{t \rightarrow \infty} y(t) = \delta$ where δ is a desired/target value. To answer, we represent the following theorem.

THEOREM 2: *Consider the LTI system as described in Eq.(3.17) for which all the assumptions mentioned in Theorem 1 are valid with the exception that $y \in \mathbb{R}^{2 \times 1}$, $C \in \mathbb{R}^{2 \times n}$, and y is such that*

$$CA^{-1} = NC \quad (3.28)$$

where $N \in \mathbb{R}^{2 \times 2}$ is of the form of a real jordan block [83] as follows:

$$N = \begin{bmatrix} \alpha & \beta \\ -\beta & \alpha \end{bmatrix} \quad (3.29)$$

with $\alpha < 0, \beta > 0$. Then it is possible to completely eliminate the effect of w on any desired output, say y_1 , and ensure $\lim_{t \rightarrow \infty} y_1(t) = \delta$ for any transients in w if the L_0 norm of u is greater than or equal to 1.

Proof: This is a scenario where C is related to CA^{-1} by a jordan block, N , which implies

the existence of complex conjugate eigenvalues in A .

Now, back to Eq.(3.17) and (3.18), for a case with two inputs and two outputs we have

$$\dot{y} = CAX + CB(u + w) \Rightarrow \begin{bmatrix} \dot{y}_1 \\ \dot{y}_2 \end{bmatrix} = CAX + CB(u + w) \quad (3.30)$$

Analogous to Eq.(3.21),

$$C = NCA \Rightarrow CA = N^{-1}C \quad (3.31)$$

Subsequently, plugging Eq.(3.31) into Eq.(3.30),

$$\begin{bmatrix} \dot{y}_1 \\ \dot{y}_2 \end{bmatrix} = N^{-1} \begin{bmatrix} y_1 \\ y_2 \end{bmatrix} + CB(u + w) \quad (3.32)$$

On the other hand, similar to Eq.(3.18), we have

$$\begin{bmatrix} y_{1_{ss}} \\ y_{2_{ss}} \end{bmatrix} = -NCB(u + w) \quad (3.33)$$

Hence, by choosing u to satisfy

$$\delta = M_1(u + w) \quad (3.34)$$

where

$$\begin{bmatrix} M_1 \\ \dots \\ M_2 \end{bmatrix} = -NCB \quad (3.35)$$

and noting that $M_1 \in \mathbb{R}^{1 \times n}$, we ensure that $\lim_{t \rightarrow \infty} y_1(t) = \delta$. This completes the proof.

◇◇◇

3.5 Problem Formulation in Frequency Domain

Since we are interested in multi-variable systems, it prompts us to formulate the problem from singular value/singular vector perspective. Specifically, it is clear that if the input vector is directed along any of the singular vectors corresponding to $\underline{\sigma} = 0$, then y would be completely isolated from the exogenous inputs. Thus, the transient control problem can be posed as follows: *Are there conditions under which it is possible to determine a singular vector corresponding to a zero singular value of the above-mentioned LTI-MISO system without the knowledge of the A matrix?*

Note: A MISO transfer function $C(sI - A)^{-1}B$ will have one or more zero singular values, i.e. $\underline{\sigma} = 0$.

THEOREM 3: *Consider the LTI system described by Eq.(3.17) and (3.18) for which all the assumptions outlined in the Theorem 1 are satisfied. If y is such that CA^{-1} and C are linearly dependent, then the direction perpendicular to CB is the direction of a singular vector corresponding to $\underline{\sigma} = 0$. Hence, if the input $(u + w)$ is directed in this direction, then y will be completely isolated from the effect of disturbance w and ensure $\lim_{t \rightarrow \infty} y(t) = 0$ for any transient in w .*

Proof: Taking Laplace transform of Eq.(3.17)

$$C(sI - A)X(s) = CB[u(s) + w(s)] \quad (3.36)$$

Therefore, from Eq.(3.21) we have,

$$\begin{aligned} (s - \frac{1}{\alpha})CX(s) &= CB[u(s) + w(s)] \Rightarrow \\ y(s) &= CB\frac{1}{(s-\frac{1}{\alpha})}[u(s) + w(s)] \end{aligned} \quad (3.37)$$

From Eq.(3.37), it can be inferred that if u is designed such that $(u(s)+w(s))$ is perpendicular to CB , then complete disturbance rejection can be achieved. This completes the proof. $\diamond\diamond\diamond$

Corollary: *For the above mentioned system under the same assumptions, any desired steady state value for the output δ can be obtained, i.e. $\lim_{t \rightarrow \infty} y(t) = \delta$.*

Proof: With,

$$CB[u(t) + w(t)] = -\delta/\alpha \quad (3.38)$$

Then referring to Eq.(3.37) We have

$$y(s) = \frac{1}{(s - 1/\alpha)}(-\frac{\delta}{\alpha})(\frac{1}{s}) \Rightarrow \lim_{t \rightarrow \infty} y(t) = \lim_{s \rightarrow 0} \frac{-\delta/\alpha}{s - 1/\alpha} = \delta \quad (3.39)$$

Remark Theorem 2 is indeed, the extension of the application of “Zero” in a multivariable system. According to the definition [84], if $G(s)$ has a zero at $s = z$, then $G(s)$ loses rank at $s = z$ and there will exist a non-zero vector u_z such that

$$G(z)u_z = 0 \quad (3.40)$$

Where u_z is called zero direction corresponding to a zero singular value of $G(z)$. Similar concept is applied in the Theorem 2; However, the approach in Theorem 2 is more broad as it works over all frequencies. In other words, the vector of inputs u corresponding to the zero singular value is shaped such that the output y tends to zero not in a certain frequency but over all range of frequencies.

3.6 Generalized Transient Control Problem for LTI Systems

Previously, to achieve a perfect transient response in output, we imposed the condition of linear dependency between C and CA which led into emergence of the output y in the expression of \dot{y} . Thereafter, we could design our control input based on the exogenous input such that the output did not react to any transient in exogenous input. To weaken this condition, we propose the following theorem:

THEOREM 4: *Consider a $[2 \times 2]$ LTI system given in Eq.(3.17) for which all the aforementioned assumptions are valid. Then by knowing A which is Hurwitz, and B and C matrices, and choosing*

$$[a_1C + CA]Bu + CB\dot{u} = 0 \quad (3.41)$$

where a_1 is the coefficient of the characteristic equation $s^2 + a_1s + a_2 = 0$, we can completely eliminate the effect of exogenous inputs w on y and ensure $\lim_{t \rightarrow \infty} y(t) = 0$ for any transients in w .

Proof: We consider the following LTI system:

$$\begin{aligned}
\dot{X} &= AX + Bu, \quad y = CX \\
\dot{y} &= C\dot{X} = CAX + CBu \\
\ddot{y} &= CA\dot{X} + CB\dot{u} = CA^2X + CABu + CB\dot{u}
\end{aligned} \tag{3.42}$$

On the other hand, according to Cayley-Hamilton theorem [83], any square matrix $A \in \mathbb{R}^{n \times n}$ satisfies its own characteristic equation, i.e.

$$\begin{aligned}
A \in \mathbb{R}^{n \times n} &\longrightarrow S^n + a_1s^{n-1} + a_2s^{n-2} + \dots + a_n = 0 \\
\Rightarrow A^n + a_1A^{n-1} + a_2A^{n-2} + \dots + a_nI &= 0 \\
\Rightarrow A^n &= -[a_1A^{n-1} + a_2A^{n-2} + \dots + a_nI]
\end{aligned} \tag{3.43}$$

Eq.(3.43) means that the n th power of any square matrix A can be expressed as a linear combination of the lower powers of A including $A^0 = I$. therefore, from Eqs.(3.42),(3.43) we have:

$$\begin{aligned}
\ddot{y} &= -(a_1CA + a_2C)X + CABu + CB\dot{u} \\
\Rightarrow \ddot{y} + a_2y &= -a_1(\dot{y} - CBu) + CABu + CB\dot{u} \\
\Rightarrow \ddot{y} + a_1\dot{y} + a_2y &= a_1CBu + CABu + CB\dot{u}
\end{aligned} \tag{3.44}$$

Therefore, by knowing A which is Hurwitz, and B and C matrices, Eq.(3.44) leads into a first order differential equation which can be solved to obtain the desired control input. In other words, by choosing u and \dot{u} such that:

$$[a_1C + CA]Bu + CB\dot{u} = 0 \tag{3.45}$$

we can guarantee complete isolation of y from the exogenous input. This completes the proof. $\diamond\diamond\diamond$

To generalize this idea to $[n \times n]$ system with characteristic equation of $S^n + a_1s^{n-1} + a_2s^{n-2} + \dots + a_n = 0$ we define:

$$O_n = \begin{bmatrix} C \\ CA \\ \vdots \\ CA^{n-1} \end{bmatrix} \quad \beta_n = \begin{bmatrix} a_{n-1} & a_{n-2} & \dots & a_0 \end{bmatrix} \quad (3.46)$$

where $O_1 = [C]$ and $O_2 = \begin{bmatrix} C \\ CA \end{bmatrix}$, and $a_0 = 1$. Therefore, considering $u^{(0)} = u$, the characteristic equation of $A \in \mathbb{R}^{n \times n}$ leads into

$$y^{(n)} + a_1y^{(n-1)} + a_2y^{(n-2)} + \dots + a_{n-1}y = \sum_{i=1}^n \beta_i O_i B u^{(n-i)}, n \geq 2 \quad (3.47)$$

Since A is Hurwitz, by choosing $RHS = 0$, it is guaranteed that $\lim_{t \rightarrow \infty} y(t) = 0$ for any transients in w . To illustrate, we consider the following system:

$$A = \begin{bmatrix} 1 & 2 \\ -4 & -3 \end{bmatrix} \quad B = \begin{bmatrix} 1 & -2 \\ -3 & 2 \end{bmatrix} \quad C = \begin{bmatrix} 2 & -1 \end{bmatrix} \quad (3.48)$$

A is Hurwitz with eigenvalues $\Lambda_{1,2} = -1 \pm 2i$ and characteristic equation is $x^2 + 2x + 5 = 0$.

Therefore, by simplifying Eq.(3.45) using values at Eq.(3.48), we have:

$$-5u_1 - 10u_2 + 5\dot{u}_1 - 6\dot{u}_2 = 0 \quad (3.49)$$

in which u_1 is considered an exogenous input and u_2 is the control input. Simulation results are depicted in Fig.3.3. it can be seen from Fig.3.3 that the output y , after reaching to steady state condition, becomes completely isolated from exogenous input u_1 .

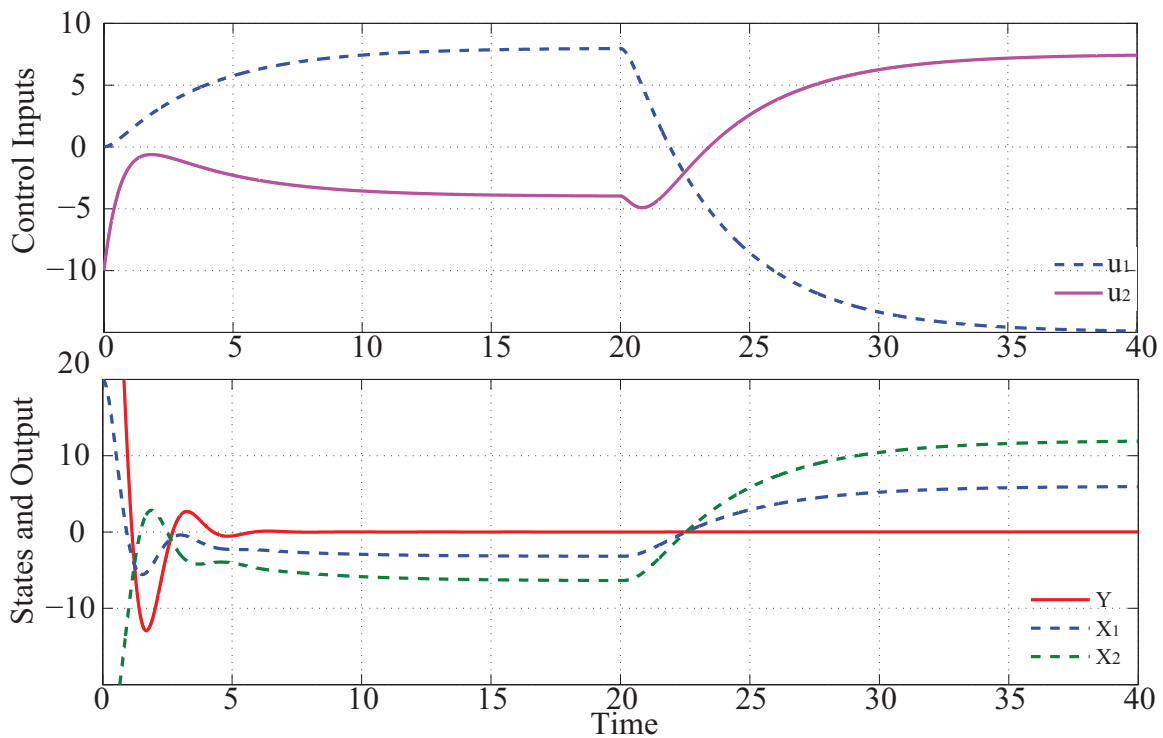


Figure 3.3: Isolation Of y From Exogenous Input u_1 using Eq.(3.44)

3.7 Transient Control in Linearized Fuel Cell Model

Here, we will represent the state space equations for the fuel cell system which will consist two inputs and one output. we define the states in terms of different mole fractions as follows:

$$Z_1 = (4\mathcal{X}_{1,a} + \mathcal{X}_{2,a} + \mathcal{X}_{4,a}), \quad Z_2 = (4\mathcal{X}_{1,r} + \mathcal{X}_{2,r} + \mathcal{X}_{4,r}) \quad (3.50)$$

Therefore, the output equation which results in utilization, in terms of states will be:

$$U = y = 1 - \frac{\dot{N}_o(t)Z_1}{\dot{N}_{in}(t)Z_2} \Rightarrow y = C(Z, t) \quad (3.51)$$

Using the pre-defined states, the state space equation of the fuel cell system will be as follows:

$$\begin{aligned} \dot{Z}_1 &= -\frac{\dot{N}_{in}(t)Z_1}{N_r(t)} + k\frac{\dot{N}_o(t)Z_2}{N_r(t)} + \frac{u_1}{N_r(t)} \\ \dot{Z}_2 &= \frac{\dot{N}_{in}(t)Z_1}{N_a(t)} - \frac{\dot{N}_o(t)Z_2}{N_a(t)} - \frac{u_2}{N_a(t)} \end{aligned} \quad (3.52)$$

$$\begin{bmatrix} \dot{Z}_1 \\ \dot{Z}_2 \end{bmatrix} = \underbrace{\begin{bmatrix} -\frac{\dot{N}_{in}(t)}{N_r(t)} & k\frac{\dot{N}_o(t)}{N_r(t)} \\ \frac{\dot{N}_{in}(t)}{N_a(t)} & -\frac{\dot{N}_o(t)}{N_a(t)} \end{bmatrix}}_{A(t)} \begin{bmatrix} Z_1 \\ Z_2 \end{bmatrix} + \underbrace{\begin{bmatrix} \frac{1}{N_r(t)} & 0 \\ 0 & -\frac{1}{N_a(t)} \end{bmatrix}}_{B(t)} \begin{bmatrix} u_1 \\ u_2 \end{bmatrix}$$

It can be seen from the above equations that fuel cell system is non-autonomous, time varying with nonlinear output. It is highly demanding to work with such a system. Hence, to simplify, we linearize the state-space equations around the steady state point as follows:

Note: The magnitude of N_a and N_r are in the same order;Thence, for simplicity we neglect their appearance in the equations.

$$\begin{aligned}\delta\dot{Z} &= A\delta Z + \delta u \\ \delta\dot{y} &= \frac{\partial C}{\partial Z}|_{ss}A\delta Z + \frac{\partial C}{\partial Z}|_{ss}\delta u\end{aligned}\tag{3.53}$$

Where $\frac{\partial C}{\partial Z}|_{ss}$ can be obtained from Eq.(3.51),

$$\frac{\partial C}{\partial Z}|_{ss} = \frac{\dot{N}_o}{\dot{N}_{in}Z_1^2} \begin{bmatrix} Z_2 & -Z_1 \end{bmatrix}\tag{3.54}$$

Plugging Eq.(3.54) into Eq.(3.53),

$$\frac{\partial C}{\partial Z}|_{ss}A = \frac{\dot{N}_o}{\dot{N}_{in}Z_1^2} \begin{bmatrix} -\dot{N}_{in}(Z_1 + Z_2) & \dot{N}_o(Z_1 + kZ_2) \end{bmatrix}\tag{3.55}$$

Now we would like to verify whether Theorem 1 can be applied to the linearized fuel cell model or not. Therefore, based on the Theorem 1, linear dependency condition similar to what was expressed earlier that needs to be satisfied to obtain perfect U response under transient conditions will be:

$$\alpha \frac{\partial C}{\partial Z}|_{ss} = \frac{\partial C}{\partial Z}|_{ss}A \Rightarrow -\alpha \frac{Z_2}{Z_1} = \frac{-\dot{N}_{in}(Z_1 + Z_2)}{\dot{N}_o(Z_1 + kZ_2)}\tag{3.56}$$

In order to be able to use theorem 1 to justify fuel cell's transient behavior, we decompose $\frac{\partial c}{\partial Z}|_{ss}A$ such that there is a linear dependent part and a perturbation part. To do that, we first build the linear dependent part from Eq.(3.56),

$$-\frac{Z_2}{Z_1} = \frac{-\dot{N}_{in}(Z_1+Z_2)}{E} \Rightarrow \quad (3.57)$$

$$E = \dot{N}_{in} \frac{Z_1}{Z_2} (Z_1 + Z_2) = \frac{\dot{N}_o}{1-y_{ss}} (Z_1 + Z_2)$$

Now we add and subtract the term $E \frac{\dot{N}_o}{N_{in} Z_1^2} \delta Z_2$ to the Eq.(3.53),

$$\delta \dot{y} = \frac{\partial C}{\partial Z} \Big|_{ss} A \delta Z + \frac{\partial C}{\partial Z} \Big|_{ss} \delta u + E \frac{\dot{N}_o}{N_{in} Z_1^2} \delta Z_2 - E \frac{\dot{N}_o}{N_{in} Z_1^2} \delta Z_2 \quad (3.58)$$

Substituting the second component of $\frac{\partial C}{\partial Z} \Big|_{ss} A \delta Z$ by $E \frac{\dot{N}_o}{N_{in} Z_1^2} \delta Z_2$ and subtracting the replaced component, we can use Eq.(3.56) and write:

$$\delta \dot{y} = \frac{\partial C}{\partial Z} \Big|_{ss} \delta Z - E \frac{\dot{N}_o}{N_{in} Z_1^2} \delta Z_2 + \frac{\dot{N}_o}{N_{in} Z_1^2} (k Z_2 + Z_1) \delta Z_2 + \frac{\partial C}{\partial Z} \Big|_{ss} \delta u \quad (3.59)$$

Similar to the Theorem 1, we factor the output out of the Eq.(3.59),

$$\delta \dot{y} = -\gamma \delta y + \underbrace{\frac{\dot{N}_o}{N_{in} Z_1^2} \left[\frac{Z_2+Z_1}{1-y_{ss}} \quad -(k Z_2 + Z_1) \right]}_P \delta Z_2 + \frac{\partial c}{\partial Z} \Big|_{ss} \delta u \quad (3.60)$$

Eventually, considering the inputs,

$$\delta \dot{y} = \underbrace{-\gamma \delta y}_{Homogeneous} + \underbrace{P \delta Z_2 + \frac{\dot{N}_o}{N_{in} Z_1^2} (Z_2 \delta u_1 - Z_1 \delta u_2)}_{Particular} \quad (3.61)$$

As γ is a positive number, similar to Theorem 1, the homogeneous part in Eq.(3.59) will attenuate as time tends toward infinity. Therefore, the question is whether the particular answer of this differential equation using control input can go toward zero or not?

Due to the existence of the perturbation term (P), the condition of Theorem 1 can not be met. However, the reason that an autonomous time-varying system such as fuel cell can have a very acceptable transient response using linear equations is that the magnitude and significance of the perturbation term in comparison with the control input term is negligible. Therefore, with designing fuel flow rate based on the current draw, a reasonably good transient response in U can be achieved.

3.8 Chapter Summary

In this Chapter, a method for controlling transient response of the output of a system for which sensing or accurate estimation was assumed not to be available, and comprehensive information regarding plant was not reachable was proposed. First, the area from where this problem was raised was described. Then it was shown through both analysis and simulation that under certain conditions, perfect disturbance attenuation is possible. The method was then verified in frequency domain as well. Thereafter, the conditions under which transient control was possible were relaxed and a more general Theorem was expressed and proved. At the end, the approach was applied to fuel cell and similarity and differences were discussed. It was shown that even though fuel cell system is nonlinear, and time-varying, a linear system approach can still be applied yielding a reasonable transient response for the output.

CHAPTER 4

DECENTRALIZED CONTROL FOR A FUEL CELL HYBRID POWER NETWORK

1

4.1 Chapter Overview

This chapter addresses development of decentralized control scheme for a simple hybrid power system consisting of a single fuel cell and an ultra-capacitor. This work develops separate controllers for the fuel cell and the ultra-capacitor, rather than a centralized controller. With a goal of developing a control paradigm that is scalable to many energy resources connected to a network, the controllers are designed primarily to use locally sensed information. Explicit communication between controllers, such as exchange of locally sensed information, is absent. An energy conservation based approach, combined with a current regulation method developed by the authors in their earlier work [3], is used for transient control of the fuel cell. The control of state-of-charge of the ultra-capacitor is also principally governed by energy conservation, but implemented using two different approaches. One is based on dissipation, and the other is based on voltage modulation. The former is a conser-

¹The contents of this chapter have been previously published [85, 40].

vative approach, while the latter is potentially more energy efficient. Simulation as well as experimental results are presented to demonstrate these concepts.

4.2 Hybrid Network and Control Objectives

Fig. 4.1 is a schematic of the hybrid system with a decentralized control scheme. Other approaches for building a fuel cell ultra-capacitor/battery are presented in [10, 12, 35, 86, 87, 3]. In our approach, we assume that fuel cell and the ultra-capacitor are connected in parallel.

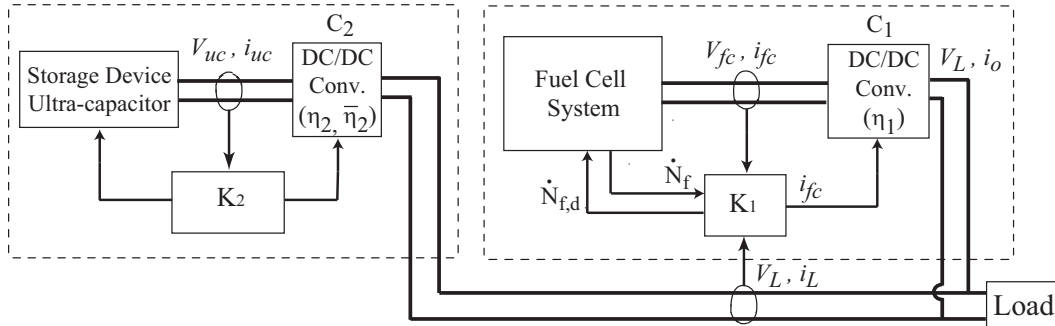


Figure 4.1: Schematic of Hybrid Fuel Cell System with Decentralized Control

Using a uni-directional DC/DC converter C_1 , the fuel cell supplies power to the load. The ultra-capacitor is connected to the load through a bi-directional DC/DC converter C_2 allowing charge and discharge. Referring to Fig.4.1, Some features of the hybrid system are:

1. Due to their fast responses, C_1 and C_2 are assumed to be static energy conversion devices, with C_1 having an efficiency of η_1 and C_2 having discharge and charge efficiencies of η_2 and $\bar{\eta}_2$ respectively [88, 8]. These efficiencies are bounded, but unknown and time-varying. We also assume that $\eta_{2,min} \leq \eta_2, \bar{\eta}_2 \leq \eta_{2,max}$. Furthermore, we consider

C_1 to be operating in current control mode, while C_2 maintains voltage V_L in a voltage control mode.

2. Based on the schematic in Fig.4.1, since the fuel cell and the ultra-capacitor are connected in parallel, the following is true at any instant:

$$V_L i_L = \eta_1 V_{fc} i_{fc} + \left[\frac{\eta_2 + \bar{\eta}_2}{2} + \frac{\eta_2 - \bar{\eta}_2}{2} \text{sgn}(i_{uc}) \right] V_{uc} i_{uc} \Rightarrow \begin{cases} V_L i_L = \eta_1 V_{fc} i_{fc} + \eta_2 V_{uc} i_{uc}, & i_{uc} > 0 \\ V_L i_L = \eta_1 V_{fc} i_{fc} + \bar{\eta}_2 V_{uc} i_{uc}, & i_{uc} < 0 \end{cases} \quad (4.1)$$

where $i_{uc} > 0$ and $i_{uc} < 0$ imply charge and discharge respectively of the capacitor. The above equation implies that the net power demand $V_L i_L$ is supplied at every instant.

3. To realize a decentralized control, we impose the following restrictions on K_1 and K_2 . Controller K_1 uses measurements of V_{fc} , V_L , i_L , and \dot{N}_f , commands C_1 to draw i_{fc} , and commands the FSS to deliver a desired fuel flow rate of $\dot{N}_{f,d}$. However, K_1 does not use measurements of i_{uc} , V_{uc} or η_2 . This is also indicated in Fig.4.1.
4. As shown in Fig.4.1, controller K_2 measures V_{uc} and i_{uc} only, and does not use measurements of V_L , i_L , V_{fc} , i_{fc} or η_1 . K_2 commands C_2 to maintain a desired V_L .

4.2.1 Control Objectives

Referring to Fig.4.1, and under the operational conditions in section 4.2, the control objectives are:

1. The target fuel utilization at steady state will be $U_{ss} = 0.8$, and the deviations from U_{ss} during transients should be minimized [3, 1].
2. Control scheme is designed to maintain the SOC of the ultra-capacitor at the target value of S_t .
3. Control the load voltage V_L around a nominal value.

4.3 Decentralized Control Using Conservation of Energy Principle

4.3.1 Approach

This work applies conservation of energy to develop decentralized control of the hybrid system in Fig.4.1. Conceptually, the approach is illustrated in Fig. 4.2.

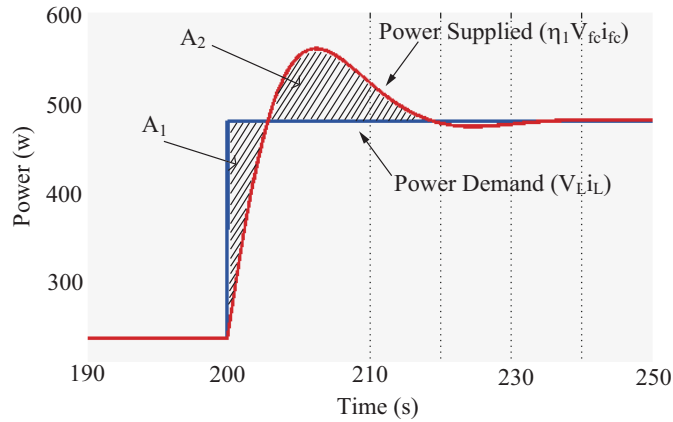


Figure 4.2: Conservation of Energy Approach

The figure shows a step increase in power demand $V_L i_L$ and the corresponding load-following response of the source (fuel cell, $\eta_1 V_{fc} i_{fc}$). The area A_1 represents the energy supplied by the storage device (ultra-capacitor in this case) to make up for the fuel cell's

deficiency in load following mode. Therefore, if the area A_2 , which represents the extra energy supplied by the FC, match A_1 , then not only the load is met, but also the capacitor will be charged to its original SOC in ideal scenario. Extending this idea, in the transient response of the SOFC, we denote $A_{1,j} = 1, 2, \dots$ as the areas where the ultra-capacitor is discharged and $A_{2,q} = 1, 2, \dots$ as the areas where the ultra-capacitor is charged. Then under ideal charge/discharge, i.e. $\eta_2 = \bar{\eta}_2 = 1$, the condition

$$\lim_{t \rightarrow \infty} E_A = \lim_{t \rightarrow \infty} \left(\sum_j A_{1,j} - \sum_q A_{2,q} \right) \rightarrow 0 \quad (4.2)$$

ensures the storage element maintains its original energy level at steady-state. Ideally, the above condition can be fulfilled by K_1 without any information about the capacitor by just ensuring

$$\lim_{t \rightarrow \infty} \int_0^t \Delta P dt = 0, \quad \Delta P \triangleq (V_L i_L - \eta_1 V_{fc} i_{fc}) \quad (4.3)$$

In the presence of losses in C_2 with discharge and charge efficiencies η_2 and $\bar{\eta}_2$ respectively, Eq.(4.2) is modified to

$$\lim_{t \rightarrow \infty} E_A = \lim_{t \rightarrow \infty} \left(\sum_i \frac{A_{1,i}}{\eta_2} - \sum_k \frac{A_{2,k}}{\bar{\eta}_2} \right) \rightarrow 0. \quad (4.4)$$

If we assume η_2 and $\bar{\eta}_2$ to be known then, using ΔP as defined in Eq.(4.3), Eq.(4.4) is satisfied by K_1 by ensuring

$$\lim_{t \rightarrow \infty} I_e = 0, \quad I_e \triangleq \int_0^t \left[\frac{\eta_2^{-1} + \bar{\eta}_2^{-1}}{2} + \frac{\eta_2^{-1} - \bar{\eta}_2^{-1}}{2} \text{sgn}(\Delta P) \right] \Delta P dt \quad (4.5)$$

where $\text{sgn}(\cdot)$ denotes signum function. However, η_2 and $\bar{\eta}_2$ will be unknown to K_1 . Therefore, we need to build a robust control around this principle to handle such uncertainty in a decentralized manner. The next sections will demonstrate the validity of the main principle.

4.3.2 Implementation and Simulations

To demonstrate that energy conservation can be used in principle to design decentralized control, we consider a simplified scenario. We assume that in addition to the local information mentioned in Assumption 2, controller K_1 has exact knowledge of η_2 and $\bar{\eta}_2$. Next, in designing K_1 , we recall that the commanded i_{fc} must be based on the actual fuel flow \dot{N}_f for transient control of U , as detailed in [3]. Also, \dot{N}_f is driven by the demanded fuel $\dot{N}_{f,d}$, which in turn is determined from $i_{fc,d}$. Thus, the command i_{fc} to C_1 is determined as follows:

$$\dot{N}_{f,d} = \frac{i_{fc,d} \mathcal{N}_{cell}}{4nFU_{ss}} \beta \Rightarrow i_{fc} = \frac{4nFU_{ss} \dot{N}_f}{\mathcal{N}_{cell} \beta}, \quad (4.6)$$

where $\beta = [1 - (1 - U_{ss})k]$. From Eq.(4.6) we note that designing K_1 reduces to the design of the reference $i_{fc,d}$. The design of $i_{fc,d}$ is based on the following observation: In load-following mode, the fuel cell provides the entire power demand at steady-state and uses

transient perturbations in power to regulate the ultra-capacitor SOC. With this goal, and incorporating the approach outlined in section 4.3.1, we formulate $i_{fc,d}$ as:

$$i_{fc,d} = \frac{V_L i_L}{\eta_1 V_{fc}} + g_i I_e, \quad k_i > 0 \quad (4.7)$$

where I_e is defined in Eq.(4.5) and g_i is the integral gain. This design is implemented and simulation results are summarized in Fig.4.3. The parameter values chosen are

$$C = 25\text{F}, \eta_1 = 0.8, \eta_2 = \bar{\eta}_2 = 0.8, g_i = 0.01 \quad (4.8)$$

The power demand $V_L i_L$ is subjected to step changes. We note that K_2 simply maintains the constant voltage V_L across the load. Fig.4.3(a) confirms the control of SOC and Fig.4.3(b) plots $V_L i_L$ and $\eta_1 V_{fc} i_{fc}$.

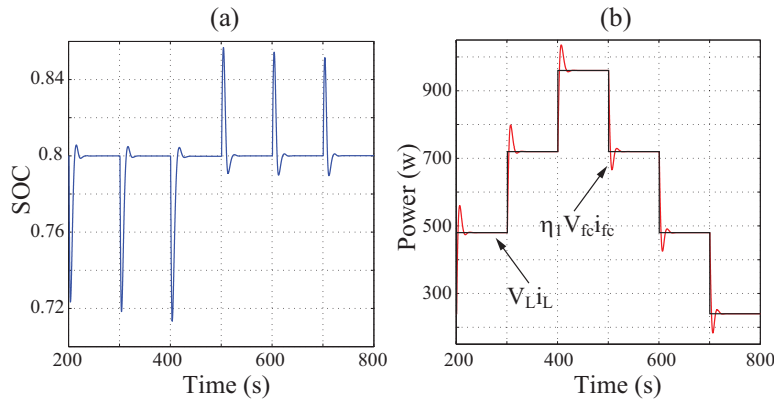


Figure 4.3: Energy Conservation based Control with Known η_2 and $\bar{\eta}_2$

4.4 Decentralized Control Design

4.4.1 Design of K_1 using a Lower Bound on η_2 and $\bar{\eta}_2$

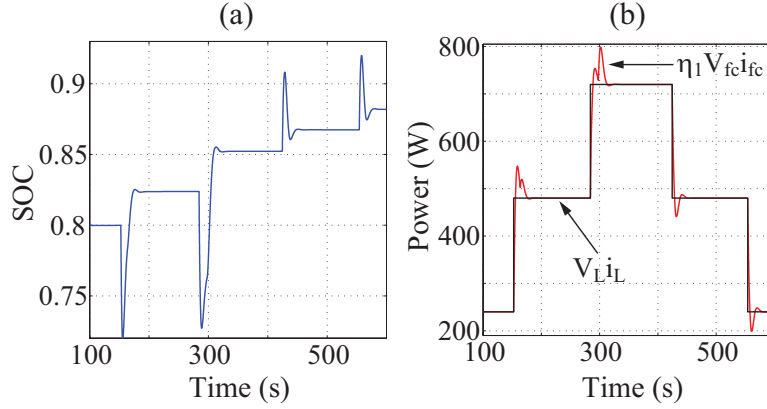


Figure 4.4: Energy Conservation with a Conservative Estimate of η_2 and $\bar{\eta}_2$

Next consider a more realistic case where K_1 has no knowledge of η_2 and $\bar{\eta}_2$ but knows a lower bound $\eta_{2,min} \leq \eta_2, \bar{\eta}_2$. Accordingly, in Eq.(4.7), instead of using I_e from Eq.(4.5), a conservative I_e is used as shown

$$I_e \triangleq \int_0^t \left[\frac{\eta_{2,min}^{-1} + \eta_{2,min}}{2} + \frac{\eta_{2,min}^{-1} - \eta_{2,min}}{2} \text{sgn}(\Delta P) \right] \Delta P dt \quad (4.9)$$

Simulation results with I_e calculated using Eq.(4.9) are shown in Fig.4.4. The parameter values chosen were same as in Eq.(4.8). Additionally, $\eta_{2,min} = 0.7$ was chosen.

The conservative nature of this approach can be inferred from Fig.4.4(a) where the SOC builds up with changes in power demand. The power demand and supplied power are plotted together in Fig.4.4(b). Therefore, we now have a conservative control K_1 which will gradually lead to over-charging the ultra-capacitor. Since we consider the energy storage

device to be of finite capacity, we must regulate the SOC. To address this in a decentralized manner two approaches are discussed in subsequent sections.

4.4.2 Dissipation Based Approach for Designing K_2

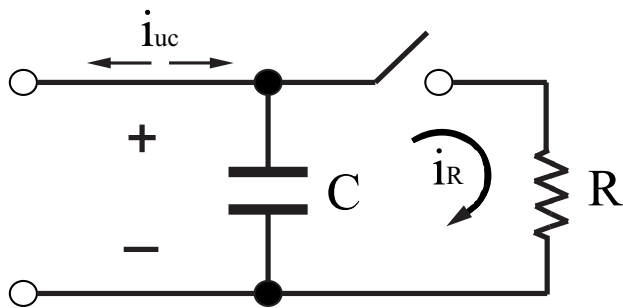


Figure 4.5: Dissipation Circuit Schematic

One way to regulate the ultra-capacitor's SOC is to dissipate the extra energy through a variable resistance connected to the ultra-capacitor. Granted that this would lead to additional energy loss, but it is a simple yet effective way to control the SOC. The configuration for dissipation is shown in Fig.4.5 which is a resistance in parallel with capacitor allowing K_2 to handle the charge-discharge in a decoupled manner. The energy dissipation can be controlled by K_2 by actuating the switch shown in both configurations in Fig.4.5, e.g. using pulse-width-modulation (PWM). Since the SOC is a local information for K_2 , charge management is done locally without any information about the fuel cell. The following equation represents case (a) in Fig. 4.5:

$$C\dot{V}_{uc} = -(i_{uc} + i_R), \quad \dot{V}_{uc} = -\frac{1}{C}(i_{uc} + V_{uc}\sigma_R) \quad (4.10)$$

where σ_R is the effective conductance that can be varied by changing the duty cycle of switching. We assume $R = 25\Omega$, and hence

$$\begin{aligned} \text{duty cycle} = 0 &\Rightarrow \sigma_R = 0 \\ \text{duty cycle} = 1 &\Rightarrow \sigma_R = 0.04 \end{aligned} \tag{4.11}$$

4.4.2.1 First Order Controller - P Type

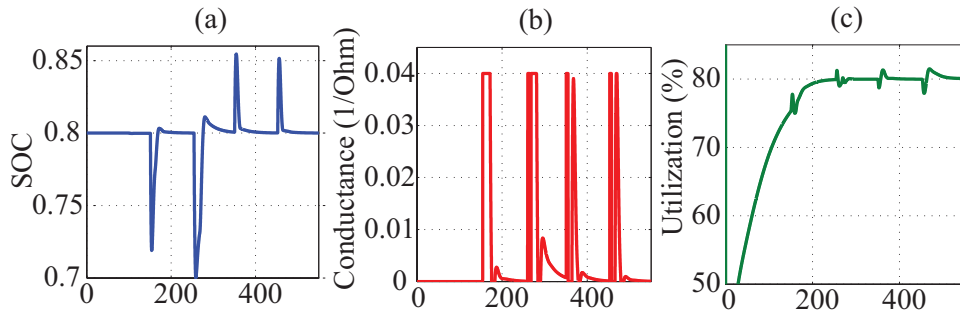


Figure 4.6: System response with a P controller for dissipation

The objective here is to maintain the ultra-capacitor's SOC around a desired value which is 0.8 in this case. In other words, we need to have an exponential decay toward a desired voltage ($V_{uc,d}$) using the Eq. 4.10. Thence, we need to design the conductance of the resistor so that:

$$i_{uc} + V_{uc}\sigma_R = g_p(V_{uc} - V_{uc,d}) \quad , g_p > 0 \tag{4.12}$$

Eq. 4.12 guarantees that the ultra-capacitor's voltage tends to the desired value using an adjustable proportional controller whose gain is set to $g_p = 0.01$ in this case. Finally,

solving for σ_R in Eq. 4.12,

$$\sigma_R = g_p \left(1 - \frac{V_{uc,d}}{V_{uc}}\right) - \frac{i_{uc}}{V_{uc}} \quad (4.13)$$

Using the Eq. 4.13, Fig. 4.6 shows that state of charge returns to the desired value within a reasonable time after the load is implemented no matter step changes are positive or negative. Not to mention, saturation limits of 0 and 0.04 have been imposed to conductance to make sure first the resistance does not go to negative values as it does not have any physical meaning. Furthermore, to ensure resistance does not go to infinity, saturation limits needs to be enforced.

4.4.2.2 PI Controller

The objective here is to treat σ_R as a control input and to design a control law that will stabilize the equilibrium $V_{uc} = V_{uc,d}$ and $V_{uc,d}$ is such that $V_{uc,d}/V_{uc,max} = 0.8$. For our ultra-capacitor, $V_{uc,max} \approx 16V$ and hence $V_{uc,d} = 13V$. Since for constant load under steady-state $i_{uc} = 0$, a proportional controller of the form $\sigma_R = [g_{p,uc}(V_{uc} - V_{uc,d}) - i_{uc}]/V_{uc}$ will suffice. However, a PI controller will better perform under load variations. Hence, the following PI control law is proposed:

$$\sigma_R = \frac{g_{p,uc}}{V_{uc}}(V_{uc} - V_{uc,d}) + \frac{g_{i,uc}}{V_{uc}} \int_0^t (V_{uc} - V_{uc,d}) dt \quad (4.14)$$

Results for step changes is depicted in Fig.4.7. In contrast to Fig.4.4(a) where the SOC control was not implemented in K_2 , the SOC converges to 0.8 with the PI control of Eq.(4.14) implemented in K_2 . The manner in which the resistance R is used in the PI control is evident from Fig.4.7(b).

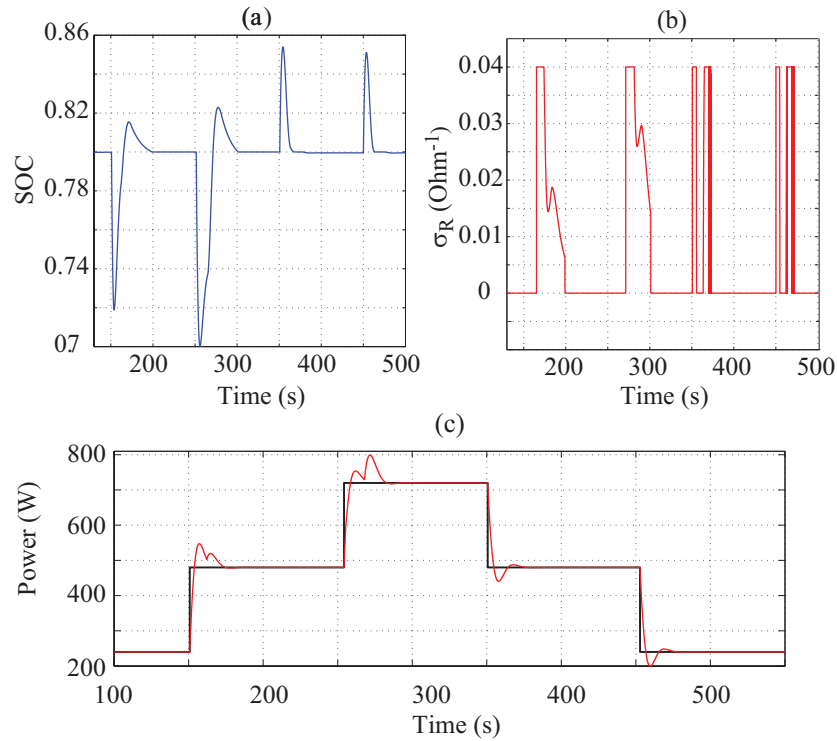


Figure 4.7: System response with a PI controller for dissipation

The integrator is also held once upper saturation in σ_R is reached from below or lower saturation is reached from above. Also, it can be observed that as SOC drops below 0.8, the resistance switches off and when it exceeds 0.8, the resistance becomes effective.

Comparing Fig. 4.6 (a) and Fig. 4.7(a), it can be seen that SOC returns to desired value to some extent faster using the PI controller. Although the amount of over charge is relatively

more in the second order case, the dissipation phenomenon takes place faster using the PI controller. The pattern with which the resistance is used in the P and PI controller is demonstrated in Fig. 4.6 (b) & Fig. 4.7(b) respectively. Saturation limits are visible in the picture namely 0 and 0.04. It can be inferred from the graphs that as SOC drops below 0.8, the resistance switches off and as it passes beyond 0.8, resistance becomes effective.

4.4.2.3 Frequency Domain Analysis for PI Controller

Note that in Eq.(4.14), we did not incorporate i_{uc} , which is a local information and can be measured. The main reason for this is that we want σ_R to primarily respond to changes in V_{uc} and not respond to perturbations in i_{uc} . Thus, i_{uc} can be considered as a disturbance input in Eq.(4.10). Note also that in load-following mode, i_{uc} would be close to zero and hence the noise-to-signal ratio of its measurement is expected to be high, especially when load variations are gradual. Since the change in SOC is expected to be a gradual process, we want σ_R to respond only to the low frequency component of V_{uc} . Hence, $k_{p,uc}$ and $k_{i,uc}$ should be tuned to low values so that closed-loop dynamics is slower compared to the dynamics of i_{fc} .

Leaving aside the high frequency noise, it is expected that the frequency content $\Omega_{i_{uc}}$ of i_{uc} to consist of the frequency content of i_L and that of i_{fc} . This is evident from Eq.(4.1). Considering a controller $D(s)$ connected in series to the plant $G(s) = -1/(Cs)$

and a standard negative feedback loop, one can write

$$\begin{aligned}
 E(s) &= \frac{1}{1+L(s)}V_{uc,d}(s) + \frac{G(s)}{1+L(s)}i_{uc}(s) \\
 E(s) &\triangleq (V_{uc,d}(s) - V_{uc}(s)), \quad L(s) = D(s)G(s)
 \end{aligned} \tag{4.15}$$

where, the control input is $i_R = V_{uc}\sigma_R$. Since $V_{uc,d}$ is a constant, reference tracking, disturbance rejection and noise rejection can be simultaneously achieved by the PI controller proposed in Eq.(4.14), which translates into $D(s) = g_{p,uc} + g_{i,uc}/s$ in frequency domain.

With this configuration, the loop gain $L(s) = D(s)G(s)$ is already high at low frequencies and low at high frequencies; Moreover, the zero at $(\frac{-g_{i,uc}}{g_{p,uc}})$ can be tuned to obtain a desirable roll off. Furthermore, attenuation of i_{uc} is achieved at low frequencies due to $|L(j\omega)| \gg |G(j\omega)|$, and at high frequencies due to $|G(j\omega)| \rightarrow 0$.

4.4.3 Voltage Regulation Based Approach for K_2

Using dissipation for controlling the SOC is based on the premise that extra energy will be lost. The main idea in the voltage regulation method is to prevent this loss. Note that energy loss would be prevented if the fuel cell controller K_1 has accurate knowledge of η_2 and $\bar{\eta}_2$. Hence, the objective of this design is to develop a mechanism by which the fuel cell can learn the aforementioned efficiencies without direct sensing or communication with K_2 . To this end, we propose the following approach. As mentioned in section 4.2, K_2 can manipulate V_L . Therefore K_2 can manipulate V_L based on the SOC. As charge builds up, V_L can be increased gradually by K_2 . Not only will it regulate V_{uc} , but since V_L is a global

variable, the fuel cell can simultaneously use the low frequency component of V_L to improve its lower bound $\eta_{2,min}$.

Load fluctuation is an undesirable phenomenon in the power networks. Therefore, the aforementioned voltage regulation method, even though is capable of inducing the fuel cell to improve its $\eta_{2,min}$ estimate, must be designed in a way such that voltage fluctuations are low and they diminish as the estimate of $\eta_{2,min}$ improves. The voltage was modulated using an integrator

$$V_L = 24 + g_{i,vr} \int_0^t (V_{uc} - V_{uc,d}) dt, \quad (4.16)$$

with $g_{i,vr} = 0.005$ for a test simulation. Moreover, as soon as the low frequency component of SOC is sufficiently close to 0.8, the integrator resets V_L to 24V. That results in a saw-tooth type of response as shown in Fig.4.8(a). On the other hand, at the fuel cell side, an integrator is used which is similar to Eq.(4.16) to utilize the load deviations from 24V for efficiency estimation.

$$\eta_{2,min}(t) = \eta_{2,min}(0) + g_{i,vr} \int_0^t (V_L - 24) dt \quad (4.17)$$

Results are depicted in Fig.4.8 demonstrating the response using the above mentioned I-controllers in both K_1 and K_2 sides. In this simulation pulsed changes power demand were applied every 200s.

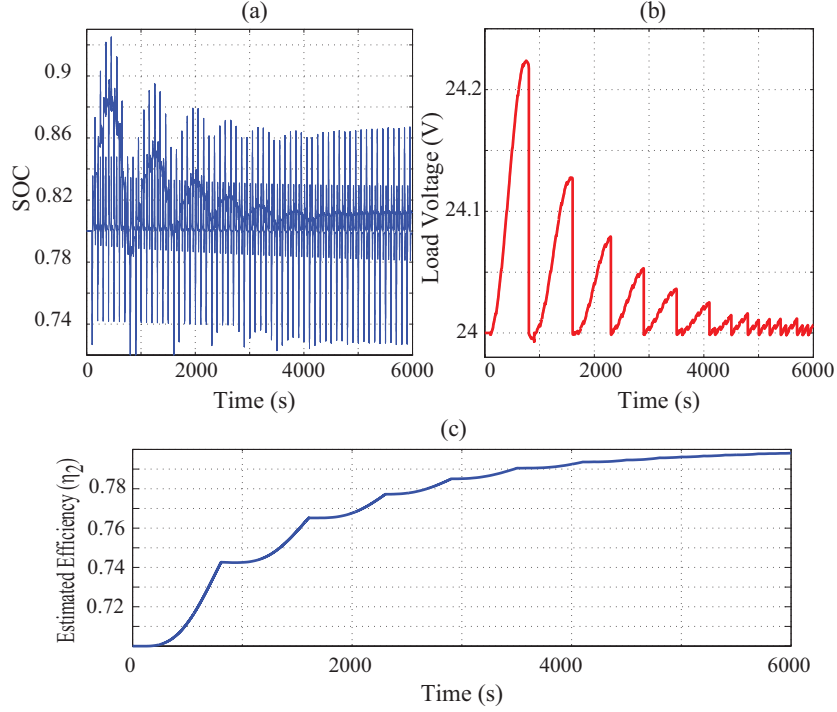


Figure 4.8: Simulations with Voltage Modulation and Efficiency Estimation

From Fig.4.8(a), it is clear K_2 is able to maintain the SOC through voltage modulation. Further, Fig.4.8(b) shows that voltage fluctuations reduce over time. This is primarily due to better estimation of $\eta_{2,min}$ by K_1 over time. The estimation is depicted in Fig.4.8. Another observation is that at the beginning which corresponds to higher SOC fluctuations, efficiency learning was fast. However, its speed decreased as time proceeded. The estimation process therefore requires not only the voltage modulation but also requires persistent perturbations in the power demand.

4.5 Experimental Results

The theoretical framework developed for the decentralized control in [85] is further validated by an experimental setup. This goal was achieved using a “hardware in the loop” test bench of the emulated fuel cell along with an ultra capacitor, an electronic load and two DC-DC converters of suitable rating and adjustability which are all shown in Fig.4.9.

Table 4.1: Equipment specifications

item	Spec.(V)	Spec.(i)	Make
dSpace	i/p:120V AC	-	dSpace1103
Power Supply	110V AC/DC	o/p:50A	Ametek SGA100/50
Electronic Load	i/p:120V AC	0-120A	Sorenson SLH
Ultracapacitor(250F)	16.2V DC	2000A	BMOD0250 P16
Unidirectional Converter	44-50V DC	40A	Zahn DC-5050F-SU
Bidirectional Converter	44-50V DC	40A	Zahn DC-5050F-SU
Current Sensors	-	1-100A	Fluke-80i-110S
Voltage Sensors	0-1KV	10mA	Resistance Divider

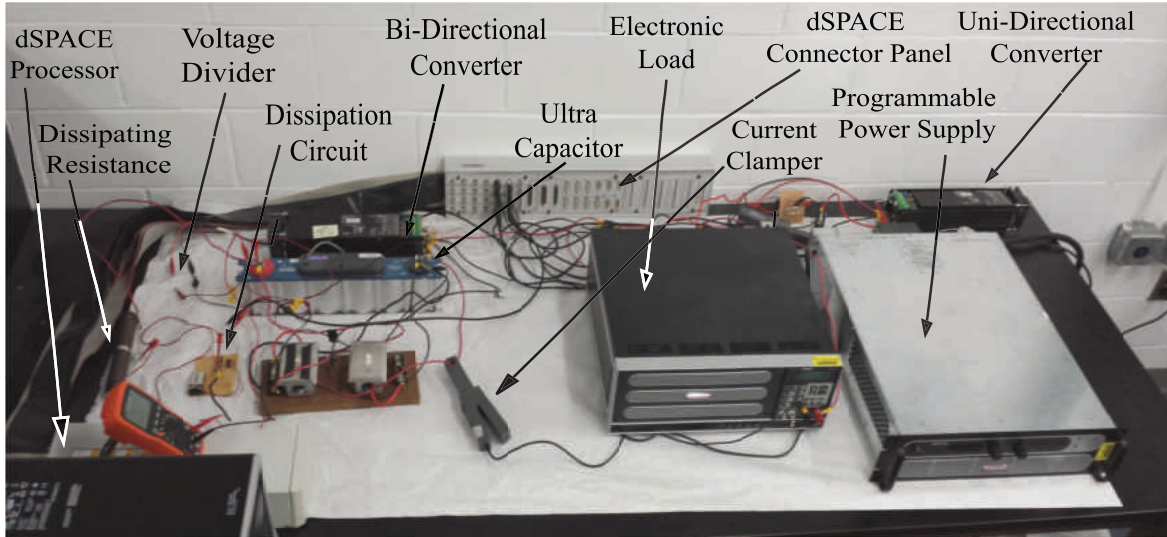


Figure 4.9: Experimental Test Stand

Furthermore, the technical specification of each equipment in Fig.4.9 is presented in Table 4.1.

The experimental SOFC system which we employed is in fact a real time emulation of the mathematical model of the SOFC developed in [1], through a Matlab interface to the dSpace 1103 digital platform. The emulation scheme is essentially performed by commanding the programmable power supply voltage in such a fashion that is mandated by SOFC model. The current flowing out of the power supply is then sensed and fed back to the SOFC model for error correction purposes.

4.5.1 Dissipation Based Approach

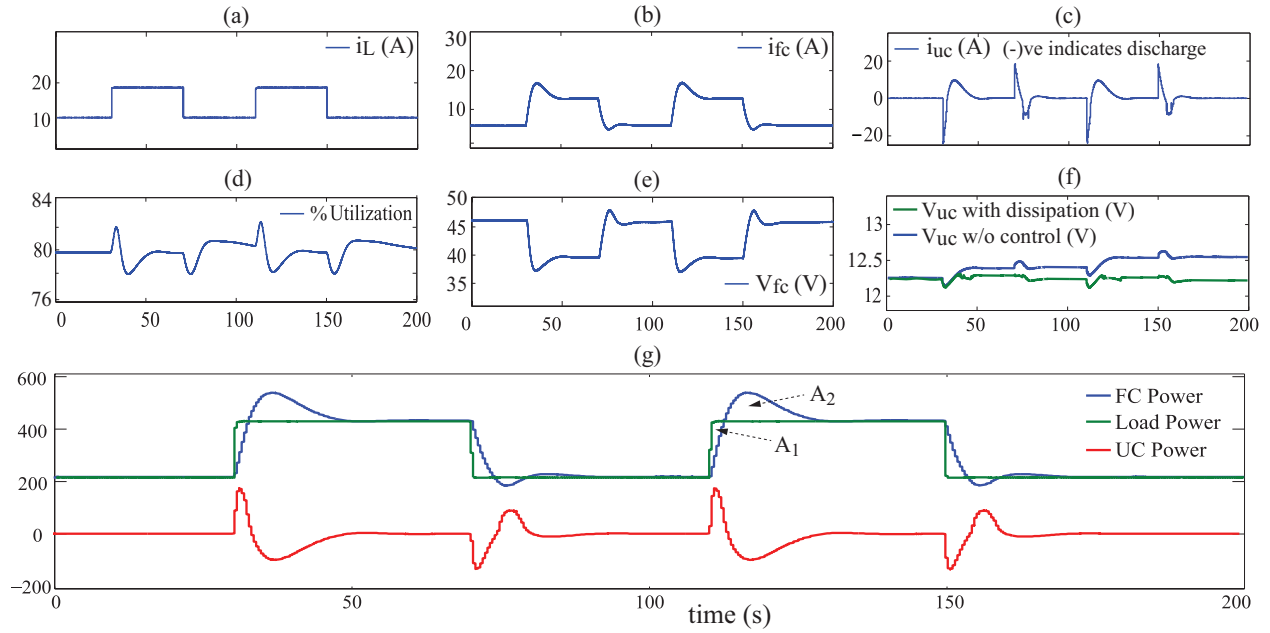


Figure 4.10: Experimental Results for Dissipation Based Approach

This approach which was described in section 4.4.2 has been implemented to the test stand and the results are depicted in Fig.4.10. The conservative nature of the approach is illustrated in Fig.4.10(d) along with a controlled SOC level maintained at 0.75. As is shown in Fig.4.10(b), a repetitive step load change from 10A level to 20A level has been implemented to the system by effectively varying the load resistance from 2.4Ω to 1.2Ω and vice versa. The slow response of the FC to the load changes, along with UC's contribution to make up for FC's deficiency during load transients is visible in Fig.4.10(b). Fig.4.10(a) not only proves that the objective regarding keeping $U_{ss} = 0.8$ is satisfied, it makes the role of PWM circuit in controlling UC Voltage stand out.

4.5.2 Voltage regulation approach

To implement this method which essentially results in an adaptive control like approach, the effectiveness of this method improves with repeated load fluctuations, that can be considered similar to “persistent excitations.” Such persistent fluctuations leads to improved estimates of converter efficiencies. The response of system is shown in Fig.4.11.

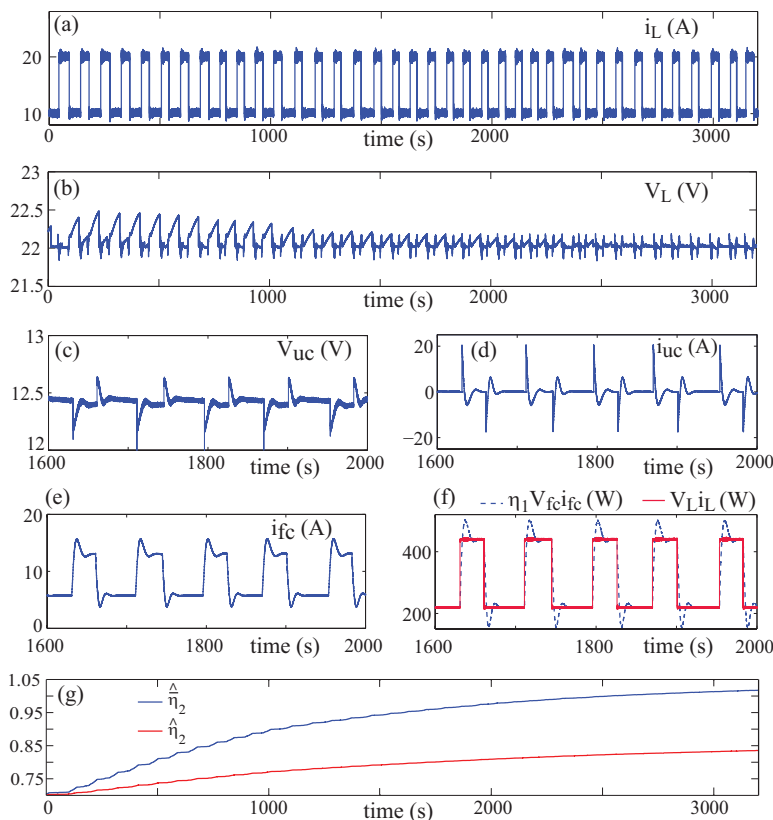


Figure 4.11: Experimental Results for Voltage Regulation Based Approach-Powers

It can be inferred from Fig.4.11 that load voltage fluctuations imposed by controller K_2 diminish over time starting from $\sim 0.5V$ and leveling out at $< 0.05V$. Moreover, with a closer look at UC voltage, it is observed that the amount of overcharge in UC decreases

with time. Moreover, it shows how FC and UC respond to a Load current change. Fig.4.11 also represents how FC provides extra power to make up for energy loss in UC. Overall, it can be inferred from the curves that the system performance improves over time.

The estimation of η_2 and $\bar{\eta}_2$ has also been depicted in Fig.4.11. The initial guess for both of them was set to be $\eta_{2,min}(0) = 0.7$. As is visible from the graph, the discharge efficiency $\eta_2 \simeq 0.84$, and charge efficiency $\bar{\eta}_2 > 1$. It can be seen that the estimation process is designed such that while η_2 is getting estimated, the estimation for $\bar{\eta}_2$ is halted, and while $\bar{\eta}_2$ is calculated, the other one is stopped.

4.6 OBSERVATIONS

4.6.1 Overall System Loss Trends

While both approaches described above perform satisfactorily in terms of meeting the control objectives, they have certain advantages and disadvantages which makes each approach appealing from different perspectives. The voltage regulation based approach progressively reduces energy losses; yet it relies on persistent excitation of the load to improve its efficiency estimates. On the other hand, the dissipation based approach results in uniform energy loss, but it does not require perturbations on the network. The energy losses with each approach were compared and plotted in Fig.4.12. Each data point represents an average power loss over an interval, calculated as

$$W_{loss,i} = \frac{1}{t_i - t_{i,0}} \int_{t_{i,0}}^{t_i} (V_L i_L - V_{fc} i_{fc}) dt \quad (4.18)$$

for both approaches. In Eq.(4.18), $\Delta t_i = t_i - t_{i,0}$ represents the i^{th} interval ending at t_i and starting at $t_{i,0}$. Each interval is roughly the same, around 100s, consisting of one step-up and one step-down in i_L . The final instants t_i were not all equispaced in time. For example, $(t_5 - t_4)$ and $(t_7 - t_6)$ are longer than the others. It can be observed from the plot that with voltage regulation, the losses decay over time whereas it is uniform for the dissipation based approach. The overall magnitudes are not considerably different. This is because the changes in capacitor voltage due to overcharging (and hence the required dissipation) were low in our experiments, owing to a high capacity of 250F and comparatively lower power levels, see Fig.4.10(f). It is expected that with lower capacity storage the advantages of voltage regulation will be more prominent.

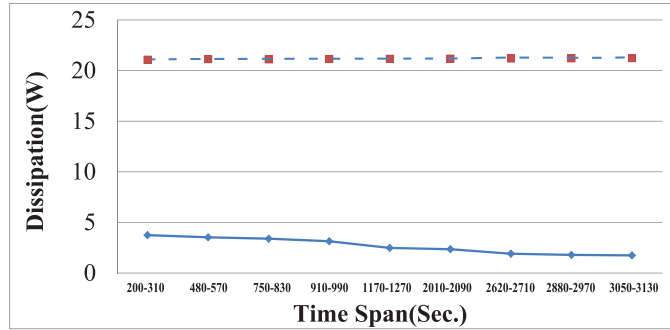


Figure 4.12: Power Loss Trends with Voltage Regulation and Dissipation Approaches

4.6.2 Comparison between Centralized and Decentralized Strategies

As discussed in the Introduction, one advantage of the decentralized approach is fault tolerance. This is illustrated here for the hybrid SOFC system through a simple observation. Referring to previous centralized control in [3], the fuel cell current demand $i_{fc,d}$, which is

one control input, was designed as

$$i_{fc,d} = \frac{V_L i_L}{\bar{\eta}_1 V_{fc}} + g(E_s) + \delta_1(E_s) \quad (4.19)$$

where, $E_s = S - S_t$, S is the SOC of the ultra-capacitor. The function g and the switching parameter δ_1 are both dependent on E_s . However in the decentralized approach proposed in the paper, $i_{fc,d}$ is designed as given in Eq.(4.7), where the integral I_e is defined in Eq.(4.5). It is clear from the above two equation that, in centralized case, the control input $i_{fc,d}$ depends on the SOC, whereas in the latter, the control input is independent of SOC. Therefore, in the event of a fault in the ultra-capacitor or a fault in sensing the SOC, $i_{fc,d}$ will drive an incorrect SOFC current demand in the centralized control. This in turn will affect the SOFC's fuel flow rate, its delivered power and cause potential depletion or overcharge of the ultra-capacitor. In contrast, in the decentralized controller the invariance of $i_{fc,d}$ to SOC will prevent capacitor and thereby system damage. It is however pointed out that the effectiveness of the decentralized approach over centralized control is also dependent on the nature of faults. For certain faults the advantage may be clear, while for others secondary protection will be necessary for both approaches.

4.7 Area Matching Using Dynamic Response of System

In this section, the possibility of implementing a feed forward control scheme using the same conservation of energy principle discussed in previous chapter will be addressed. Here, the objective is to come up with a family of solutions for controllers through which

the dynamic response of the system will result in a shape for which the summation of areas above and beneath the load line cancel out each other; i.e. the SOC of the capacitor is preserved while load is met and fuel utilization of FC is kept within the safe range.

4.7.1 Second Order Under-damped Systems

Referring to Fig.4.2, one could argue that the hybrid system response to step change in load resembles that of a second order under-damped system. This resemblance motivated us to investigate whether we can implement the idea of conservation of energy through an alternative approach. Therefore, we first aimed to obtain the conditions under which the step response of a second order under-damped system can ensure area matching.

Consider the following second order equation of motion:

$$\ddot{X} + 2\zeta\omega_n\dot{X} + \omega_n^2X = u(t) \quad (4.20)$$

where $0 \leq \zeta < 1$ is the damping ratio and ω_n is the natural frequency of the system. The solution of the above differential equation to a unit step input yields [89],

$$X(t) = \frac{1}{\omega_n^2} \left[1 - e^{-\zeta\omega_n t} \left(\cos \omega_d t + \frac{\zeta}{\sqrt{1-\zeta^2}} \sin \omega_d t \right) \right] \quad (4.21)$$

where $\sigma = \zeta\omega_n$. Therefore, to implement the method proposed in section 4.3.1, we need to make sure that the following integral diminishes as time tends toward infinity.

$$\lim_{t \rightarrow \infty} \int_0^t [X(t) - X_{ss}] dt \rightarrow 0 \implies A_1 - A_2 \rightarrow 0 \quad (4.22)$$

Applying Eq.(4.21) into Eq.(4.22), and normalize it with respect to steady state response X_{ss} ,

$$I = \int_0^\infty \frac{1}{\omega_n^2} [-e^{-\sigma t} (\cos \omega_d t + \frac{\zeta}{\sqrt{1-\zeta^2}} \sin \omega_d t)] \quad (4.23)$$

which simplifies into:

$$-\omega_n^2 I = \int_0^\infty e^{-\sigma t} [\cos \omega_d t] dt + \frac{\sigma}{\omega_d} \int_0^\infty e^{-\sigma t} [\sin \omega_d t] dt \quad (4.24)$$

To ensure the area matching and conservation of energy, Eq.(4.24) needs to be equal to zero.

After simplifying Eq.(4.24) using integral tables, we have:

$$\frac{\sigma}{\omega_d^2 + \sigma^2} + \frac{\sigma}{\omega_d} \frac{\omega_d}{\omega_d^2 + \sigma^2} = 0 \implies 2 \frac{\zeta}{\omega_n} = 0 \quad (4.25)$$

Eq.(4.25) shows that the only system whose response to a step function can guarantee the area matching and conservation of energy is a system with no damping. This is quite obvious as such system has a sinusoidal response to a step function which means the summation of areas over and under the step will cancel each other out. Therefore, higher order solutions

could be sought as an alternative for area matching and conservation of energy method. Further work in this regards is to be pursued in the future.

4.8 Chapter Summary

A decentralized control approach was developed for a solid oxide fuel cell system hybridized with an ultra-capacitor in parallel. In the decentralized framework, there are individual controllers for the fuel cell and the ultra-capacitors that do not explicitly communicate with each other but use local information for control. However, the system as a whole satisfies the control objectives without jeopardizing any component. A conservation of energy based approach for control was developed. First, a conservative approach was taken to design the decentralized scheme. This approach was extended to a voltage modulation method which essentially imposed energy conservation on the energy storage device and simultaneously provided a means for implicit communication between the controllers using the power line itself. To extend this research in future, a network with more than two elements and eventually, a network consisting of multiple elements will be attempted. The general observation is that migrating to a decentralized control involves a trade-off between the advantage gained through reduced computation and sensing, with the need for adding a dissipation mechanism or the need for adding an extra capability in power conversion like voltage modulation.

CHAPTER 5 CONCLUSIONS

In this work, a method for controlling transient response of the output of a system for which sensing or accurate estimation was assumed not to be available and comprehensive information regarding plant was not reachable was proposed. First, the area from where this problem was raised was described. Then it was shown through both analysis and simulation that under certain conditions, perfect disturbance attenuation is possible. The method was then verified in frequency domain as well. Thereafter, the conditions under which transient control was possible were relaxed and a more general Theorem was expressed and proved. At the end, the approach were related to fuel cell and similarity and differences were discussed. It was shown that even though fuel cell system is nonlinear, and time-varying, a linear system approach can still be applied yielding a reasonable transient response for the output.

Moreover, A decentralized control approach was developed for a solid oxide fuel cell system hybridized with an ultra-capacitor in parallel. In the decentralized framework, there are individual controllers for the fuel cell and the ultra-capacitors that do not explicitly communicate with each other but use local information for control. However, the system as a whole satisfies the control objectives without jeopardizing any component. A conservation of energy based approach for control was developed. First, a conservative approach was taken

to design the decentralized scheme. This approach was extended to a voltage modulation method which essentially imposed energy conservation on the energy storage device and simultaneously provided a means for implicit communication between the controllers using the power line itself. To extend this research in future, a network with more than two elements and eventually, a network consisting of multiple elements will be attempted. The general observation is that migrating to a decentralized control involves a trade-off between the advantage gained through reduced computation and sensing, with the need for adding a dissipation mechanism or the need for adding an extra capability in power conversion like voltage modulation.

Furthermore, The decentralized control framework developed by the authors in [85] has been further validated using an experimental setup. A few adjustments were made to the theory to make it compatible based on the practical limitations of our experimental setup. However, we preserve the main conservation of energy based method for decentralized control. Moreover, a detailed stability analysis was provided to confirm the performance of the framework. Both dissipation based and voltage regulation based decentralized controllers were tested and validated. The notable observation from the experiments was that the overall system efficiency improves for the voltage regulation approach with time, whereas the dissipative approach, while being simpler, results in a recurring but limited power loss in the system. This is an expected phenomena as the voltage regulation method results in adaptive learning of efficiencies, which over times improves in the presence of repeated

fluctuations in load and therefore the conservative approach described in section 4.4.1 evolves as the exact approach and the over-charging of the ultra-capacitor diminishes over time.

LIST OF REFERENCES

- [1] T. Das, S. Narayanan, and R. Mukherjee, “Steady-state and transient analysis of a steam-reformer based solid oxide fuel cell system,” *Journal of Fuel Cell Science and Technology*, vol. 7, FEB 2010. ASME International Mechanical Engineering Congress and Exposition, Seattle, WA, NOV 11-15, 2007.
- [2] T. Allag and T. Das, “Robust nonlinear control of fuel cell ultra-capacitor hybrid system,” in *American Control Conference*, pp. 6923–6929, 2010.
- [3] T. Allag and T. Das, “Robust control of solid oxide fuel cell ultra-capacitor hybrid system,” *IEEE Transactions on Control Systems Technology*, vol. 20, pp. 1–10, January 2012.
- [4] J. Larminie and A. Dicks, *Fuel Cell Systems Explained*. John Wiley and Sons Ltd, 2003.
- [5] X. Li, *Principles of Fuel Cells*. Taylor and Francis Group, 2006.
- [6] K. Yasuda and T. Ishii, “Basic concept and decentralized autonomous control of super-distributed energy systems,” *Electrical Engineering in Japan*, vol. 151, no. 1, pp. 43–55, 2005.
- [7] J. R. Meacham, F. Jabbari, J. Brouwer, J. L. Mauzey, and G. S. Samuelsen, “Analysis of stationary fuel cell dynamic ramping capabilities and ultra capacitor energy storage using high resolution demand data,” *Journal of Power Sources*, vol. 156, no. 2, pp. 472 – 479, 2006.
- [8] T. Das and S. Snyder, “Robust adaptive control of solid oxide fuel cell ultra-capacitor hybrid systems,” *IEEE Transactions on Control Systems Technology*, vol. 21, no. 2, 2013.
- [9] R. Gaynor, F. Mueller, F. Jabbari, and J. Brouwer, “On control concepts to prevent fuel starvation in solid oxide fuel cells,” *Journal of Power Sources*, vol. 180, pp. 330–342, 2008.
- [10] A. Drolia, P. Jose, and N. Mohan, “An approach to connect ultracapacitor to fuel cell powered electric vehicle and emulating fuel cell electrical characteristics using switched mode converter,” in *Industrial Electronics Society, 2003. IECON '03. The 29th Annual Conference of the IEEE*, vol. 1, pp. 897 – 901 vol.1, 2-6 2003.

- [11] P. Thounthong, S. Rael, and B. Davat, "Control strategy of fuel cell/supercapacitors hybrid power sources for electric vehicle," *Journal of Power Sources*, vol. 158, no. 1, pp. 806 – 814, 2006.
- [12] A. Vahidi, A. Stefanopoulou, and H. Peng, "Current management in a hybrid fuel cell power system: A model-predictive control approach," *Control Systems Technology, IEEE Transactions on*, vol. 14, pp. 1047 –1057, nov. 2006.
- [13] F. Mueller, J. Brouwer, F. Jabbari, and S. Samuelsen, "Dynamic simulation of an integrated solid oxide fuel cell system including current-based fuel flow control," *Journal of Fuel Cell Science and Technology*, vol. 3, no. 2, pp. 144–154, 2006.
- [14] W. Schmittinger and A. Vahidi, "A review of the main parameters influencing long-term performance and durability of pem fuel cells," *Journal of Power Sources*, vol. 180, no. 1, pp. 1 – 14, 2008.
- [15] F. Mueller, F. Jabbari, and J. Brouwer, "On the intrinsic transient capability and limitations of solid oxide fuel cell systems," *Journal of Power Sources*, vol. 187, no. 2, pp. 452 – 460, 2009.
- [16] F. Mueller, F. Jabbari, R. Gaynor, and J. Brouwer, "Novel solid oxide fuel cell system controller for rapid load following," *Journal of Power Sources*, vol. 172, no. 1, pp. 308 – 323, 2007. {ACS} San Francisco 2006 Fuel and Cell Symposium. American Chemical Society National Meeting. San Francisco, {CA} Sept 10-14 2006.
- [17] C. Stiller, B. Thorud, O. Bolland, R. Kandepu, and L. Imsland, "Control strategy for a solid oxide fuel cell and gas turbine hybrid system," *Journal of Power Sources*, vol. 158, no. 1, pp. 303–315, 2006.
- [18] M. H. Nehrir and C. Wang, *Modeling and Control of Fuel Cells - Distributed Generation Applications*. John Wiley and Sons, Inc., 2009.
- [19] A. K. M. M. Murshed, B. Huang, and K. Nandakumar, "Estimation and control of solid oxide fuel cell system," *Computers and Chemical Engineering*, vol. 34, pp. 96–111, 2010.
- [20] S. Campanari, "Thermodynamic model and parametric analysis of a tubular sofc module," *Journal of Power Sources*, vol. 92, no. 1-2, pp. 26 – 34, 2001.
- [21] A. Lazzaretto, A. Toffolo, and F. Zanon, "Parameter setting for a tubular sofc simulation," *JOURNAL OF ENERGY RESOURCES TECHNOLOGY-TRANSACTIONS OF THE ASME*, vol. 126, pp. 40–46, MAR 2004.
- [22] K. Sedghisigarchi and A. Felachi, "Control of grid-connected fuel cell power plant for transient stability enhancement," *Proceedings of the IEEE Power Engineering Society Transmission and Distribution Conference*, vol. 1, pp. 383–388, January 2002.

- [23] M. Nayeripour, M. Hoseintabar, and T. Niknam, “A new method for dynamic performance improvement of a hybrid power system by coordination of converter’s controller,” *Journal of Power Sources*, vol. 196, no. 8, pp. 4033 – 4043, 2011.
- [24] S. A. Hajimolana and M. Soroush, “Dynamics and control of a tubular solid oxide fuel cell,” *Industrial & Engineering Chemistry Research*, vol. 48, p. 61126125, 2009.
- [25] R. Kandepu, L. Imsland, B. A. Foss, C. Stiller, B. Thorud, and O. Bolland, “Modeling and control of a soft-gt-based autonomous power system,” *ENERGY*, vol. 32, pp. 406–417, APR 2007. 18th International Conference on Efficiency, Costs, Optimization, Simulation, and Environmental Impact of Energy Systems, Trodheim, NORWAY, JUN 22-24, 2005.
- [26] A. Reinert and T. Strohbach, “Determination of the global/local fuel utilization via variation of the fuel utilization,” *ECS Transactions*, vol. 25, no. 2(1), pp. 811 – 814, 2009.
- [27] H. Gorgun, M. Arcaç, S. Varigonda, and S. A. Bortoff, “Observer designs for fuel processing reactors in fuel cell power systems,” *International Journal of Hydrogen Energy*, vol. 30, pp. 447–457, 2005.
- [28] J. T. Pukrushpan, A. G. Stefanopoulou, and H. Peng, *Control of Fuel Cell Power Systems: Principles, Modeling, Analysis, and Feedback Design*. Advances in Industrial Control, London: Springer, 2004.
- [29] V. Tsourapas, A. G. Stefanopoulou, and J. Sun, “Model-based control of an integrated fuel cell and fuel processor with exhaust heat recirculation,” *IEEE Transactions on Control Systems Technology*, vol. 15, no. 2, pp. 233–245, 2007.
- [30] Y. Guezennec, T. Choi, G. Paganelli, and G. Rizzoni, “Supervisory control of fuel cell vehicles and its link to overall system efficiency and low-level control requirements,” in *Proceedings of the American Control Conference*, pp. 2055–2061, Ohio State University, AACC, June 2003.
- [31] M. Grujicic, K. M. Chittajallu, and J. T. Pukrushpan, “Control of the transient behaviour of polymer electrolyte membrane fuel cell systems,” *PROCEEDINGS OF THE INSTITUTION OF MECHANICAL ENGINEERS PART D-JOURNAL OF AUTOMOBILE ENGINEERING*, vol. 218, pp. 1239–1250, NOV 2004.
- [32] J. Sun and I. V. Kolmanovsky, “Load governor for fuel cell oxygen starvation protection: a robust nonlinear reference governor approach,” *IEEE Transactions on Control Systems Technology*, vol. 13, pp. 911 – 920, nov. 2005.
- [33] C. H. Woo and J. Benziger, “{PEM} fuel cell current regulation by fuel feed control,” *Chemical Engineering Science*, vol. 62, no. 4, pp. 957 – 968, 2007.

- [34] A. Vahidi and W. Greenwell, “A decentralized model predictive control approach to power management of a fuel cell-ultracapacitor hybrid,” in *American Control Conference, 2007. ACC '07*, pp. 5431–5437, july 2007.
- [35] A. Arce, A. J. del Real, and C. Bordons, “MPC for battery/fuel cell hybrid vehicles including fuel cell dynamics and battery performance improvement,” *Journal of Process Control*, vol. 19, no. 8, pp. 1289–1304, 2009.
- [36] S. Espiari and M. Aleyaasin, “Transient response of pem fuel cells during sudden load change,” in *Energy Conference and Exhibition (EnergyCon), 2010 IEEE International*, pp. 211–216, 2010.
- [37] D. Bhattacharyya and R. Rengaswamy, “A review of solid oxide fuel cell (SOFC) dynamic models,” *Industrial and Engineering Chemistry Research*, vol. 48, no. 13, pp. 6068–6086, 2009.
- [38] B. Huang, Y. Qi, and M. Murshed, “Solid oxide fuel cell: Perspective of dynamic modeling and control,” *Journal of Process Control*, vol. 21, pp. 1426–1437, 2011.
- [39] H. Xi, S. Varigonda, and B. Jing, “Dynamic modeling of a solid oxide fuel cell system for control design,” in *American Control Conference (ACC), 2010*, pp. 423–428, June 2010.
- [40] O. Madani, A. Bhattacharjee, and T. Das, “Decentralized power management in a hybrid fuel cell ultra-capacitor system,” *Submitted to IEEE Transactions on Control Systems Technology*, 2014.
- [41] A. E. Auld, K. M. Smedley, F. Mueller, J. Brouwer, and G. S. Samuelson, “Load-following active power filter for a solid oxide fuel cell supported load,” *Journal of Power Sources*, vol. 195, no. 7, pp. 1905–1913, 2010.
- [42] P. Thounthong, S. Rael, and B. Davat, “Utilizing fuel cell and supercapacitors for automotive hybrid electrical system,” in *Applied Power Electronics Conference and Exposition, 2005. APEC 2005. Twentieth Annual IEEE*, vol. 1, pp. 90–96 Vol. 1, 2005.
- [43] M. Y. Ayad, M. Becherif, A. Djerdir, and A. Miraoui, “Sliding mode control for energy management of dc hybrid power sources using fuel cell, batteries and supercapacitors,” in *Clean Electrical Power, 2007. ICCEP '07. International Conference on*, pp. 500–505, 21-23 2007.
- [44] A. Payman, S. Pierfederici, and F. Meibody-Tabar, “Energy Management in a Fuel Cell/Supercapacitor Multisource/Multiload Electrical Hybrid System,” *IEEE TRANSACTIONS ON POWER ELECTRONICS*, vol. 24, pp. 2681–2691, DEC 2009.

- [45] Z. Jiang, L. Gao, and R. A. Dougal, “Adaptive control strategy for active power sharing in hybrid fuel cell/ battery power sources,” *IEEE Transactions on Energy Conversion*, vol. 22, no. 2, pp. 507–515, 2007.
- [46] P. Thounthong, S. Rael, and B. Davat, “Energy management of fuel cell/battery/supercapacitor hybrid power source for vehicle applications,” *JOURNAL OF POWER SOURCES*, vol. 193, pp. 376–385, AUG 1 2009.
- [47] V. Paladini, T. Donato, A. de Risi, and D. Laforgia, “Super-capacitor fuel-cell hybrid electric vehicle optimization and control strategy development,” *Energy Conversion and Management*, vol. 48, pp. 3001–3008, 2007.
- [48] M. Uzunoglu and M. S. Alam, “Dynamic modeling, design and simulation of a pem fuel cell/ultracapacitor hybrid system for vehicular applications,” *Energy Conversion and Management*, vol. 48, pp. 1544–1553, 2007.
- [49] A. Hajizadeh and M. A. Golkar, “Intelligent power management strategy of hybrid distributed generation system,” *International Journal of Electrical Power*, vol. 29, no. 10, pp. 783 – 795, 2007.
- [50] T. Das and S. Snyder, “Adaptive control of a solid oxide fuel cell ultra-capacitor hybrid system,” in *American Control Conference (ACC), 2011*, pp. 3892 –3898, 29 2011-july 1 2011.
- [51] P. Adhikari and M. Abdelrahman, “Modeling, control, and integration of a portable solid oxide fuel cell system,” *Journal of Fuel Cell Science and Technology*, vol. 9, no. 1, p. 011010, 2012.
- [52] A. Y. Sendjaja and V. Kariwala, “Decentralized control of solid oxide fuel cells,” *Industrial Informatics, IEEE Transactions on*, vol. 7, no. 2, pp. 163–170, 2011.
- [53] L. Bakule, “Decentralized control: An overview,” *Annual Reviews in Control*, vol. 32, no. 1, pp. 87 – 98, 2008.
- [54] M. M. Haddad, Q. Hui, V. Chellaboina, and S. G. Nersesov, “Hybrid decentralized maximum entropy control for large-scale dynamical systems,” in *American Control Conference, 2006*, pp. 6 pp.–, 2006.
- [55] A. Ramakrishna and N. Viswanadham, “Decentralized control of interconnected dynamical systems,” in *Decision and Control including the Symposium on Adaptive Processes, 1980 19th IEEE Conference on*, pp. 538–543, Dec 1980.
- [56] Y. Guo, D. J. Hill, and Y. Wang, “Nonlinear decentralized control of large-scale power systemsq,” *Automatica*, 2000.

- [57] V. Ugrinovskii and H. Pota, “Decentralized control of power systems via robust control of uncertain markov jump parameter systems,” in *Proceedings of 43rd IEEE Conference on Decision and Control*, pp. 3503–3508, University of New South Wales, IEEE, December 2004.
- [58] A. Aquino-Lugo, *Distributed and decentralized control of the power grid*. PhD thesis, University of Illinois at Urbana-Champaign, 2011.
- [59] A. Tuladhar, K. Jin, T. Unger, and K. Mauch, “Parallel operation of single phase inverter modules with no control interconnections,” in *Applied Power Electronics Conference and Exposition, 1997. APEC '97 Conference Proceedings 1997., Twelfth Annual*, vol. 1, pp. 94–100 vol.1, Feb 1997.
- [60] P. Hines and S. Talukdar, “Reciprocally altruistic agents for the mitigation of cascading failures in electrical power networks,” in *Infrastructure Systems and Services: Building Networks for a Brighter Future (INFRA), 2008 First International Conference on*, pp. 1–6, Nov 2008.
- [61] D. Chiappini, A. L. Facci, L. Tribioli, and S. Ubertini, “Soft management in distributed energy systems,” *Journal of Fuel Cell Science and Technology*, vol. 8, no. 3, p. 031015, 2011.
- [62] A. K. Saha, S. Chowdhury, S. P. Chowdhury, and Y. H. Song, “Application of solid-oxide fuel cell in distributed power generation,” *IET Renewable Power Generation*, vol. 1, no. 4, pp. 193–202, 2007.
- [63] A. Sakhare, A. Davari, and A. Feliachi, “Fuzzy logic control of fuel cell for stand-alone and grid connection,” *Journal of Power Sources*, vol. 135, no. 12, pp. 165 – 176, 2004.
- [64] M. L. Ferrari, A. Traverso, L. Magistri, and A. F. Massardo, “Influence of the anodic recirculation transient behaviour on the soft hybrid system performance,” *JOURNAL OF POWER SOURCES*, vol. 149, pp. 22–32, SEP 26 2005.
- [65] F. P. Incropera and D. P. DeWitt, *Fundamentals of Heat and Mass Transfer*. John Wiley & Sons, Inc., fifth ed., 2002.
- [66] J. Xu and G. F. Froment, “Methane steam reforming, methanation and water-gas shift: I. Intrinsic kinetics,” *AIChE Journal*, vol. 35, no. 1, pp. 88–96, 1989.
- [67] R. Bove, P. Lunghi, and N. M. Sammes, “Soft mathematic model for systems simulations. part one: from a micro-detailed to macro-black-box model,” *International Journal of Hydrogen Energy*, vol. 30, no. 2, pp. 181 – 187, 2005.
- [68] A. Slippey, O. Madani, K. Nishtala, and T. Das, “Invariant properties in solid oxide fuel cell systems with integrated reformers,” *Submitted to International Journal of Hydrogen Energy*, 2014.

- [69] T. Bertelsen, T. Pedersen, J. Poulsen, and R. Schultz, “Modelling and optimization of solid oxide fuel cell system.” AALBORG University, 2011.
- [70] M. J. Kupilik and T. L. Vincent, “Control of a solid oxide fuel cell system with sensitivity to carbon formation,” *Journal of Power Sources*, vol. 222, no. 0, pp. 267 – 276, 2013.
- [71] P. Holtappels, L. Haart, U. Stimming, I. Vinke, and M. Mogensen, “Reaction of co/co2 gas mixtures on ni/ysz cermet electrodes,” *Journal of Applied Electrochemistry*, vol. 29, no. 5, pp. 561–568, 1999.
- [72] S. Park, J. M. Vohs, and R. J. Gorte, “Direct oxidation of hydrocarbons in a solid-oxide fuel cell,” *Nature (London)*, vol. 404, pp. 265–267, 2000.
- [73] A. Weber, B. Sauer, A. Mller, . Herbsttritt, and E. Ivers-Tiffe, “Oxidation of h2, {CO} and methane in {SOFCs} with ni/ysz-cermet anodes,” *Solid State Ionics*, vol. 152153, no. 0, pp. 543 – 550, 2002.
- [74] B. J. Spivey and T. F. Edgar, “Dynamic modeling, simulation, and {MIMO} predictive control of a tubular solid oxide fuel cell,” *Journal of Process Control*, vol. 22, no. 8, pp. 1502 – 1520, 2012. Ken Muske Special Issue.
- [75] A. Slippey, “Dynamic modeling and analysis of multiple sofc system configurations,” ms thesis, Rochester Institute of Technology, Rochester, NY, October 2009.
- [76] O. Madani and T. Das, “Transient control in multivariable systems: A study motivated by fuel cells,” in *Dynamic systems and control conference (DSCC), 2034*, 2013.
- [77] J. Klamka, *Controllability of dynamical systems*. Kluwer Academic Publishers, 1991.
- [78] D. Qiu, Q. Wang, and Y. Zhou, “Steady-state output controllability and output controllability of linear systems,” in *Computational Intelligence and Industrial Applications, 2009. PACIIA 2009. Asia-Pacific Conference on*, vol. 2, pp. 147–150, IEEE, 2009.
- [79] W. Jiang, “Output controllability of linear systems with delay,” *Journal of Mathematics for Technology*, vol. 10, pp. 1–6, 1994.
- [80] M. I. Garcia-Planas and J. L. Dominguez-Garcia, “Output controllability and steady-output controllability analysis of fixed speed wind turbine,” 2011.
- [81] M. D. Brockett, R. W .and Mesarović, “The reproducibility of multivariable systems,” *Journal of mathematical analysis and applications*, vol. 11, pp. 548–563, 1965.
- [82] M. I. Garcia-Planas, S. Tarragona, and M. Aplicada, “Analysis of functional output-controllability of time-invariant composite linear systems,” 2013.
- [83] D. Bernstein, *Matrix Mathematics: Theory, Facts, and Formulas*. Princeton university press, 2009.

- [84] S. Skogestad and I. Postlethwaite, *Multivariable Feedback Control*. Wiley, 1996.
- [85] O. Madani and T. Das, “Decentralized control of a fuel cell ultra-capacitor hybrid network,” in *American Control Conference (ACC), 2013*, pp. 5362–5367, 2013.
- [86] W. Greenwell and A. Vahidi, “Predictive control of voltage and current in a fuel cell-ultracapacitor hybrid,” *IEEE Transactions on Industrial Electronics*, vol. 57, pp. 1954–1963, 2010.
- [87] A. G. Stefanopoulou and K. Suh, “Mechatronics in fuel cell systems,” *Control Engineering Practice*, vol. 15, pp. 277–289, 2007.
- [88] S. Snyder, “Robust adaptive control for a hybrid solid oxide fuel cell system,” Master’s thesis, Rochester Institute of Technology, 2011.
- [89] K. Ogata, *Modern Control Engineering*. Upper Saddle River, NJ, USA: Prentice Hall PTR, 4th ed., 2001.